TNFα prevents FGF4-mediated rescue of astrocyte dysfunction and reactivity in human ALS models

Erika Velasquez, Ekaterina Savchenko, Sara Marmolejo-Martínez-Artesero, Désiré Challuau, Aline Aebi, Yuriy Pomeshchik, Nuno Jorge Lamas, Mauno Vihinen, Melinda Rezeli, Bernard Schneider, et al.

Neurobiology of Disease 201 (2024) 106687

Contents lists available at ScienceDirect

Neurobiology of Disease

journal homepage: www.elsevier.com/locate/ynbdi

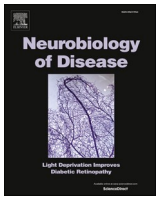

TNFα prevents FGF4-mediated rescue of astrocyte dysfunction and reactivity in human ALS models

Erika Velasquez [a,b,c,*], Ekaterina Savchenko [a,b,c], Sara Marmolejo-Martínez-Artesero [d], Désiré Challuau [d], Aline Aebi [e], Yuriy Pomeshchik [a,b,c], Nuno Jorge Lamas [f,g,h], Mauno Vihinen [i], Melinda Rezeli [j,k], Bernard Schneider [e,l], Cedric Raoul [d], Laurent Roybon [a,b,c,m,*]

[a] iPSC Laboratory for CNS Disease Modelling, Department of Experimental Medical Science, BMC D10, Lund University, 22184 Lund, Sweden
[b] Strategic Research Area MultiPark, Lund University, Lund SE-221 84, Sweden
[c] Lund Stem Cell Center, Lund University, Lund SE-221 84, Sweden
[d] INM, Univ Montpellier, INSERM, 34091, Montpellier, France
[e] Bertarelli Platform for Gene Therapy, Ecole Polytechnique Fédérale de Lausanne, Geneva, Switzerland
[f] Anatomic Pathology Service, Pathology Department, Centro Hospitalar e Universitário do Porto, Largo Professor Abel Salazar, 4099-001 Porto, Portugal
[g] Life and Health Sciences Research Institute (ICVS), School of Medicine, University of Minho, Campus de Gualtar, 4710-057 Braga, Portugal
[h] ICVS/3B's-PT Government Associate Laboratory, University of Minho, 4710-057 Braga, Portugal
[i] Department of Experimental Medical Science, BMC B13, Lund University, 22184 Lund, Sweden.
[j] Department of Biomedical Engineering, Lund University, Lund, Sweden
[k] BioMS – Swedish National Infrastructure for Biological Mass Spectrometry, Lund University, Lund, Sweden
[l] Brain Mind Institute, Ecole Polytechnique Fédérale de Lausanne, Lausanne, Switzerland
[m] Department of Neurodegenerative Science, the MiND program, Van Andel Institute, Grand Rapids, 49503, MI, USA

ARTICLE INFO

Keywords:
Amyotrophic lateral sclerosis
Induced pluripotent stem cells
Astrocytes
Fibroblast growth factor
Tumor necrosis factor-alpha
Innate immune system
Proteomics

ABSTRACT

Astrocytes play a crucial role in the onset and progression of amyotrophic lateral sclerosis (ALS), a fatal disorder marked by the degeneration of motor neurons (MNs) in the central nervous system. Although astrocytes in ALS are known to be toxic to MNs, the pathological changes leading to their neurotoxic phenotype remain poorly understood. In this study, we generated human astrocytes from induced pluripotent stem cells (iPSCs) carrying the ALS-associated A4V mutation in superoxide dismutase 1 (SOD1) to examine early cellular pathways and network changes. Proteomic analysis revealed that ALS astrocytes are both dysfunctional and reactive compared to control astrocytes. We identified significant alterations in the levels of proteins linked to ALS pathology and the innate immune cGAS-STING pathway. Furthermore, we found that ALS astrocyte reactivity differs from that of control astrocytes treated with tumor necrosis factor alpha (TNFα), a key cytokine in inflammatory reactions. We then evaluated the potential of fibroblast growth factor (FGF) 2, 4, 16, and 18 to reverse ALS astrocyte phenotype. Among these, FGF4 successfully reversed ALS astrocyte dysfunction and reactivity in vitro. When delivered to the spinal cord of the $SOD1^{G93A}$ mouse model of ALS, FGF4 lowered astrocyte reactivity. However, this was not sufficient to protect MNs from cell death. Further analysis indicated that TNFα abrogated the reactivity reduction achieved by FGF4, suggesting that complete rescue of the ALS phenotype by FGF4 is hindered by ongoing complex neuroinflammatory processes in vivo. In summary, our data demonstrate that

Abbreviations: α-amino-3-hydroxy-5-methyl-4-isoxazolepropionic acid, (AMPA); Adeno-associated virus, (AAV); Amyotrophic lateral sclerosis, (ALS); Cyclic GMP-AMP synthase - Stimulator of interferon genes, (cGAS-STING); Extracellular matrix, (ECM); Familial ALS, (fALS); Fibroblast growth factor, (FGF); Glial fibrillary acidic protein, (GFAP); Glutamate transporter-1, (GLT1); Glutamine synthetase, (GS); Green fluorescent protein, (GFP); Induced pluripotent stem cells, (iPSCs); Inhibitor of DNA binding 3, (ID3); Mitochondrial DNA, (mtDNA); Mitochondrial permeability transition pore, (mPTP); Motor neuron, (MN); Reactive oxygen species, (ROS); Spinal cord, (SC); Sporadic ALS, (sALS); Superoxide dismutase 1, (SOD1); S100 calcium binding protein beta, (S100b),; Tricarboxylic acid cycle/Electron transport chain, (TCA/ETC); Tumor necrosis factor-alpha, (TNFα); Voltage-dependent anion-selective channel 1, (VDAC1); Wildtype, (WT).

* Corresponding authors at: iPSC Laboratory for CNS Disease Modelling, Department of Experimental Medical Science, BMC D10, Lund University, 22184 Lund, Sweden; Department of Neurodegenerative Science, the MiND program, Van Andel Institute, Grand Rapids, 49503, MI, USA.

E-mail addresses: erika.velasquez@med.lu.se (E. Velasquez), ekaterina.savchenko@med.lu.se (E. Savchenko), sara.marmolejo@inserm.fr (S. Marmolejo-Martínez-Artesero), desire.challuau@inserm.fr (D. Challuau), aline.aebi@epfl.ch (A. Aebi), yuriy.pomeshchik@med.lu.se (Y. Pomeshchik), nunojlamas@med.uminho.pt (N.J. Lamas), mauno.vihinen@med.lu.se (M. Vihinen), melinda.rezeli@bme.lth.se (M. Rezeli), bernard.schneider@epfl.ch (B. Schneider), cedric.raoul@inserm.fr (C. Raoul), laurent.roybon@vai.org (L. Roybon).

https://doi.org/10.1016/j.nbd.2024.106687
Received 29 May 2024; Received in revised form 27 September 2024; Accepted 28 September 2024
Available online 1 October 2024

astrocytes generated from ALS iPSCs are inherently dysfunctional and exhibit an immune reactive phenotype. Effectively targeting astrocyte dysfunction and reactivity in vivo may help mitigate ALS and prevent MN death.

1. Background

Amyotrophic lateral sclerosis (ALS) is a fatal disorder characterized by the progressive degeneration of motor neurons (MNs) in the motor cortex, brainstem and spinal cord (SC) (Kiernan et al., 2011; Lamas and Roybon, 2021). ALS is one of the most devastating adult-onset neurodegenerative diseases, with an estimated mortality of 25,000 patients yearly in the United States (Larson et al., 2018). The disease leads to muscular weakness, atrophy, and paralysis, ultimately causing death due to respiratory failure. Most ALS cases are sporadic (sALS), but approximately 5–8 % are familial (fALS), with 15–20 % harboring a mutation in the *superoxide dismutase 1* (*SOD1*) gene (Siddique and Ajroud-Driss, 2011). The etiology of ALS remains unknown. Accumulated data suggest that glial cells are critical for disease onset and progression (Yamanaka et al., 2008), but the selective expression of mutant SOD1 in MNs does not induce neurodegeneration in mouse models, indicating active involvement of neighboring cells in ALS pathogenesis (Pramatarova et al., 2001).

In ALS, astrocytes display a neurotoxic phenotype associated with the loss of their neuro-supportive functions (Nagai et al., 2007; Tripathi et al., 2017; Di Giorgio et al., 2007). ALS astrocytes also exhibit deficits in glutamate uptake (Rothstein et al., 2005), leading to increased neurotransmitter accumulation in the synaptic cleft (Blasco et al., 2014). Mutant SOD1 astrocytes modulate the GluA2 subunit of AMPA receptors in MNs, making MNs vulnerable to glutamate excitotoxicity (Kawahara et al., 2003). The presence of reactive astrocytes has also been observed in the cortex and SC of ALS patients (Reischauer et al., 2018), releasing inflammatory and pro-apoptotic mediators that render MNs more susceptible to degeneration. Furthermore, transplanting mutant $SOD1^{G93A}$ glial-restricted precursors and human sporadic ALS spinal neural progenitor cells into the cervical SC of wildtype (WT) mice induces MN degeneration in vivo *(*Papadeas et al., *2011)*. Together, these findings indicate that astrocytes play a pivotal role in the pathogenic process underlying MN death. However, the earliest pathological changes driving astrocyte dysfunction in ALS have not been fully elucidated.

One of the challenges in understanding early molecular changes behind ALS progression is the limited access to brain samples from patients in the early stages of the disease, and the difficulty of determining the specific contribution of each cell type in complex tissues like the brain and SC. However, these challenges can be overcome by using patient-derived induced pluripotent stem cells (iPSCs). iPSC-derived astrocytes exhibit cellular pathogenic features that primarily reflect the activity of pathogenic genes or risk factors carried by the donor patient during early disease stages. Moreover, iPSC-derived astrocytes provide a platform for genetically modulating astrocyte biology, pathologic profile, and toxicity to MNs (Almad et al., 2022; Kim, 2015; Stoklund Dittlau et al., 2023; Zhao et al., 2020).

Currently, there is no effective therapy for ALS. The available pharmacological options (such as riluzole (Fang et al., 2018) or edaravone (Writing and Edaravone, 2017)), together with palliative measures, only modestly increase the life expectancy of the patients. In this context, gene therapy targeting ALS astrocytes is a potential avenue to modulate their inflammatory profile and restore their neurotrophic support. Previously, we demonstrated that treating WT astrocytes with fibroblast growth factor 2 (FGF2) increased astrocytic expression of the glutamate transporter-1 (GLT1) (Savchenko et al., 2019; Roybon et al., 2013). It has also been reported that FGF signalling in the neocortex is necessary to maintain the non-reactive state of astrocytes and accelerate their deactivation after injury (Kang et al., 2014a). These data suggest that the astrocyte FGF pathway might be a promising therapeutic target in ALS.

Here, we generated iPSCs from patients harboring mutant $SOD1^{A4V}$, and used them to investigate the earliest protein changes related to ALS progression, and how several FGF family members influence the astrocyte proteome. We found significant alterations in the levels of proteins associated with several pathways including the innate immune system, which serve as early molecular signatures of ALS astrocytes. Furthermore, we discovered that FGF4 successfully reversed ALS astrocyte dysfunction and reactivity in vitro. When delivered using AAV serotype 9 in the SC of $SOD1^{G93A}$ mice, FGF4 significantly reduced the reactivity of spinal astrocytes. However, this did not protect MNs from cell death, possibly due to ongoing complex neuroinflammatory processes in vivo.

2. Results

2.1. ALS astrocytes are dysfunctional and reactive compared to control astrocytes

We first examined whether ALS astrocytes exhibit cell-autonomous dysfunction. Astrocytes were generated from iPSCs obtained from ALS patients and healthy individuals. The ALS astrocytes carried the A4V mutation in the SOD1 protein, a variant that reduces the mean survival time to under 2 years after diagnosis (Juneja et al., 1997). After 100 days of differentiation, the astrocytes expressed canonical markers, including glial fibrillary acidic protein (GFAP), S100 calcium-binding protein beta (S100b), Ezrin, glutamine synthetase (GS), and inhibitor of DNA binding 3 (ID3). There were no significant changes observed in the percentage of astrocytic markers between control and ALS astrocytes (Fig. 1a and b). However, ALS astrocytes displayed signs of reactivity, including increased GFAP and the presence of multiple short cellular processes (Fig. 1c and d).

We next seeded 100-day-old astrocytes, maintained them in growth medium for 5 (D5) and 14 days (D14), analyzed their proteomes by mass spectrometry, and identified 7541 unique proteins (Table S1). PCA analysis showed no clear separation in the proteome profiles of control and ALS astrocytes at day 5 (D5), but indicated a trend towards separation at day 14 (D14) (Fig. S1a). We therefore conducted a sparse Partial Least Squares Discriminant Analysis (sPLS-DA) to identify specific protein signatures for control and ALS astrocytes at D5 and D14 (Fig. 1e and h). At D5, ALS and control astrocytes again grouped together, but by D14 the ALS and control astrocytes exhibited well-defined and separate profiles, reflecting time-dependent changes associated with the progression of ALS pathology (Fig. 1e). We extracted these key protein signatures and represented them in an unsupervised clustering analysis (Fig. 1h; Table S2). The cluster image map indicates that control astrocytes at D5 are distinct from ALS astrocytes in fatty acid metabolism (Cluster 1) and Clathrin-mediated endocytosis and trafficking (Cluster 2). In contrast, ALS astrocytes at D5 are marked by elevated actin stress fiber-associated protein LIMCH1 (Cluster 4). At D14, control astrocytes are distinguished in Cluster 3, which includes proteins associated with transactivation of PPRGA and ESR1, the ubiquitin-proteasome system (UPS), and the endoplasmic-reticulum-associated protein degradation (ERAD) pathway. Notably, at D14, ALS astrocytes are characterized by proteins related to the immune system, and mRNA splicing and stabilization (Cluster 5).

We also examined the particular protein changes in ALS and control astrocytes at each time point. At D5, ALS astrocytes exhibited decreased abundance of metabolic proteins (e.g., those related to amino acid and fatty acid metabolism), and increased abundance of proteins associated with the extracellular matrix (ECM) (Fig. 1f and g). The decreased abundance of metabolic proteins persisted in ALS astrocytes at D14, with additional disruption in the phagosome and vesicle transport proteins

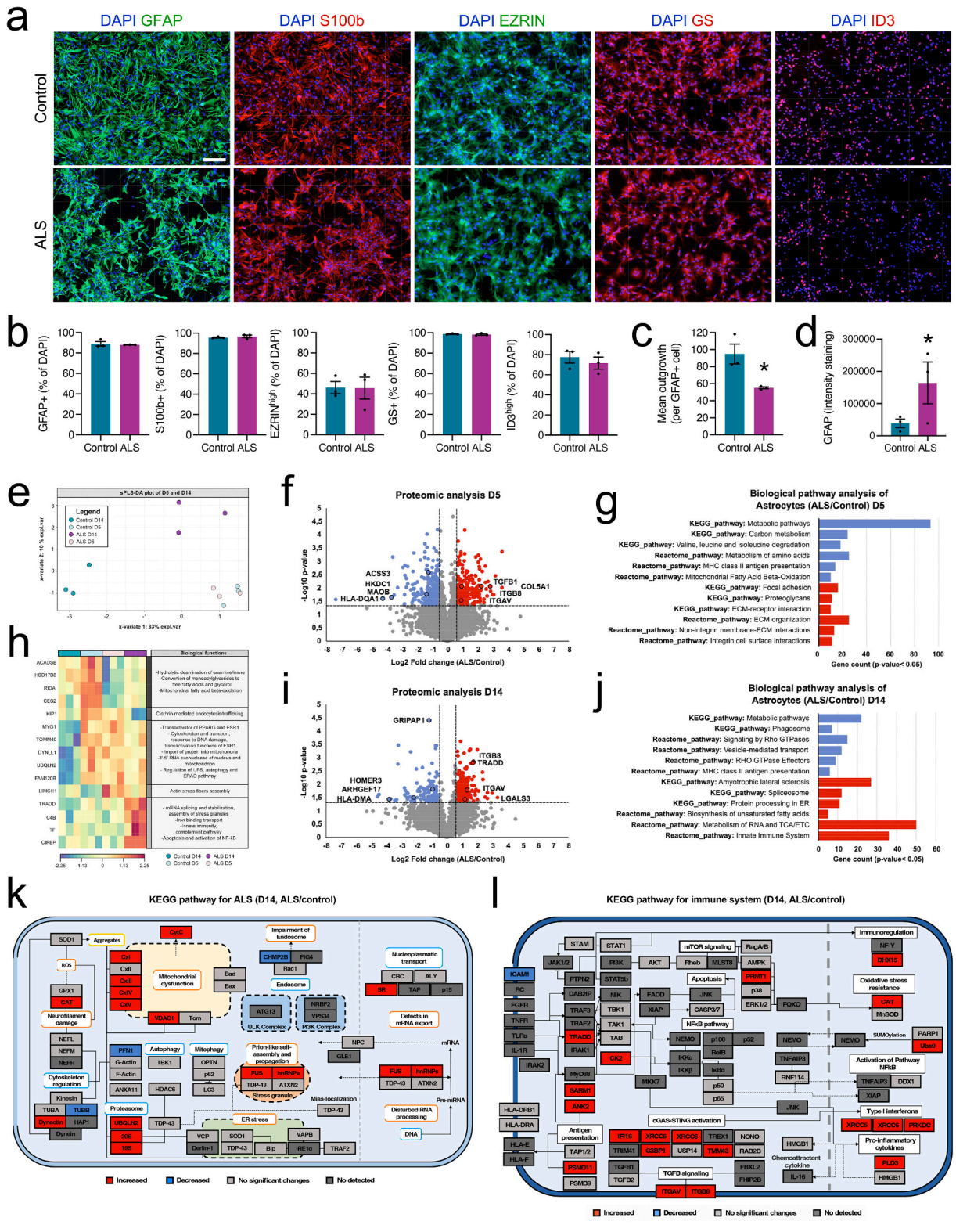

(caption on next page)

Fig. 1. a) Representative immunostaining of cultures (ALS $n = 3$, Control n = 3) for canonical astrocytic markers glial fibrillary acidic protein (GFAP), S100 calcium-binding protein beta (S100b), membrane and actin cytoskeleton linker EZRIN, glutamine synthetase (GS) and inhibitor of DNA binding 3 (ID3) at day 100. Scale bar, 100 μm.
b) Quantification of astrocytic markers in 100-day-old cultures generated from control and ALS iPSCs. Data are mean ± SEM; $n = 3$ samples per group.
c) Automated quantification of GFAP-positive cells (ALS n = 3, Control n = 3) with significant process outgrowth (in μm) using the neurite outgrowth module of MetaMorph software. Data are mean ± SEM; $n = 3$ samples per group; *t*-test, *p*-value <0.05.
d) Automated quantification of GFAP intensity staining using the multiwavelength cell scoring module of MetaMorph software. Data are mean ± SEM; $n = 3$ samples per group; t-test, *p*-value <0.05.
e) Partial Least Squares Discriminant Analysis at D5 and D14. The top 5 proteins of each component ($n = 3$ components) were selected (ALS n = 3, Control n = 3).
f) Volcano plot representing the proteins of ALS vs. control astrocytes at 5 days ((ALS n = 3, Control n = 3). Decreased and increased proteins are represented in blue and red, respectively (Two-tailed t-test *p*-value: 0.05; log2 fold-change cutoffs of +0.5).
g) Biological pathway analysis of dysregulated proteins between ALS and control astrocytes (ALS n = 3, Control $n = 3$) at 5 days (Enrichment *p*-value <0.05). Pathways derived from down and up-regulated proteins are represented in blue and red, respectively. Detriment in the metabolic pathways, including amino acids and lipids, are the main alterations observed concomitantly with the increment of proteins related to the extracellular matrix.
h) Clustering image map of the protein signatures at D5 and D14. The top 5 proteins of each component ($n = 3$ components) were represented in an unsupervised clustering analysis using Pearson's correlation distance.
i)Volcano plot representation of the proteome profile of ALS vs. control astrocytes (ALS n = 3, Control n = 3) at 14 days. Two-tailed unpaired *t*-test *p*-value: 0.05; log2 fold-change cutoffs of +0.5. Decreased and increased proteins are represented in blue and red, respectively.
j) Biological pathway analysis of dysregulated proteins in ALS vs. control astrocytes (ALS n = 3, Control n = 3) at 14 days (Enrichment *p*-value <0.05). Pathways derived from down and up-regulated proteins are represented in blue and red, respectively. The decrease of proteins in metabolic and vesicle-related pathways and the increase of proteins linked to the immune system, RNA, and TCA/ETC functions are the main findings on day 14. Additionally, from day 14, the enrichment of proteins previously associated with ALS disease starts to rise.
k) ALS mapping based on KEGG mapper color analysis. Protein abundances of ALS vs. control astrocytes (ALS n = 3, Control n = 3) at 14 days were considered in this representation (Two-tailed unpaired t-test *p*-value: 0.05; log2 fold-change cutoffs of +0.5). The ALS pathway map reveals profound alterations in themitochondrial respiratory chain complexes and the proteasome system.
l) Immune mapping based on KEGG mapper color and Reactome analysis. Protein abundances of ALS vs. control astrocytes (ALS $n = 3$, Control n = 3) at 14 days were considered in this representation (Two-tailed unpaired t-test p-value: 0.05; log2 fold-change cutoffs of +0.5). The signalling map displays a basal activation of the innate immune system in the ALS astrocytes. (For interpretation of the references to color in this figure legend, the reader is referred to the web version of this article.)

(Fig. 1i and j). At D14, we also observed an increase in proteins connected to ALS pathways, RNA and tricarboxylic acid cycle/electron transport chain (TCA/ETC) metabolism, ER protein processing, and the innate immune system (Fig. 1i and j). We then conducted a protein interaction network analysis to extract the main hubs and dissect the primary biological processes involved in ALS and innate immune pathways. We found that the ALS protein network encompassed oxidative phosphorylation, mRNA metabolism regulation, and oxidative stress response (Fig. S1b). In contrast, the innate immune system network was predominated by myeloid leukocyte activation, including the positive regulation of type I interferon production, phagocytosis, and antigen presentation (Fig. S1c).

Finally, we used the KEGG mapper to create a basic cell signalling map of ALS and immune system pathways, and identify the main proteins leading to these pathological changes. ALS mapping (Fig. 1k) revealed perturbations in mitochondrial proteins, with increased levels of respiratory complex components (CxI, CxII, CxIV, CxV), voltage-dependent anion-selective channel 1 (VDAC1), and cytochrome C. Proteins linked to the ubiquitin-proteasome system (e.g., UBQLN2) were also altered, as were known ALS pathological proteins (e.g., FUS (Kwiatkowski Jr. et al., 2009; Vance et al., 2009) and hnRNPs (Bampton et al., 2020)). The immune system mapping (Fig. 1l) showed increased levels of several proteins related to innate immune response, including the cyclic GMP-AMP synthase - Stimulator of interferon genes (cGAS-STING) pathway (Decout et al., 2021) (e.g., XRCC5, XRCC6, TMEM43), transforming growth factor beta-1 activation (i.e., ITGAV, ITGB8) and mTOR signalling (e.g., PRMT1). Together, these data indicate that ALS astrocytes exhibit time-dependent changes in their proteome profile. These changes are characterized by profound perturbations in proteins associated with mitochondrial and proteasomal functions, alongside a higher basal expression of immune-related proteins.

2.2. ALS astrocyte reactivity differs from TNFα-induced astrocyte reactivity

Tumor necrosis factor alpha (TNFα) is a cytokine that is up-regulated from the pre-symptomatic stage to the end stage in ALS patients, and in animal models of the disease (Guidotti et al., 2021). Given that ALS-astrocytes have a more pronounced pro-inflammatory profile than normal astrocytes, we therefore asked if challenging WT astrocytes with TNFα would result in the same proteome profiles observed in mutant SOD1 astrocytes. We first evaluated the effect of TNFα treatment in control and $SOD1^{A4V}$ astrocytes at D14, as this time point not only showed the most significant proteome alterations but also represents a more mature stage of astrocyte development. As expected, TNFα induced crucial inflammation-related proteins (e.g., TAP1/2, ICAM1) in both conditions (Fig. 2a; Table S2). However, ALS astrocytes had a 2- to 3-fold increase in nuclear factor kappa beta (NF-κB) and proteins related to antigen presentation (Fig. 2a). Pathway analysis also revealed that ALS astrocytes had decreased lysosome, glycan, and lipid metabolism proteins, and increased levels of cytokine signalling, ER-phagosome pathway, and proteasome proteins (Fig. 2b). ALS astrocytes also exhibited down-regulated membrane traffic, mTOR signalling, and lysosomal/peroxisomal metabolism pathways, but up-regulated immune system, cytokine, and focal adhesion pathways (Fig. 2b).

We next used hierarchical clustering (one-way ANOVA, *p*-value: 0.05; Tukeý s HSD FDR: 0.05) to compare proteome profiles of ALS and control astrocytes. The analysis revealed a high similarity in the protein clusters of TNFα-treated and non-treated ALS astrocytes (Fig. 2c). Similar results were observed for control astrocytes (Fig. 2c). In total, we identified 7 different protein clusters. Clusters 2 and 7 represent the common protein changes in ALS and control astrocytes after TNFα treatment. In Cluster 2, we found alterations in the phagosome, cell adhesion, and amino acid metabolism, while Cluster 7 encompasses proteins associated with immune activation (e.g., antigen presentation and cytokine signalling; Fig. 2d). Clusters 5 and 6 associated with ALS astrocytes regardless of treatment, and with control astrocytes after TNFα treatment (Fig. 2d). Cluster 5 exhibited downregulation of proteins involved in translation and RNA processing, while Cluster 6 comprised proteins related to the immune response, integrins, and FGF signalling (Fig. 2d). ALS and innate immune system mapping showed that TNFα treatment only induced a few additional proteins in ALS astrocytes (e.g. cytoskeletal, endosome, antigen presentation, and apoptosis proteins (Figs. 2e and f).

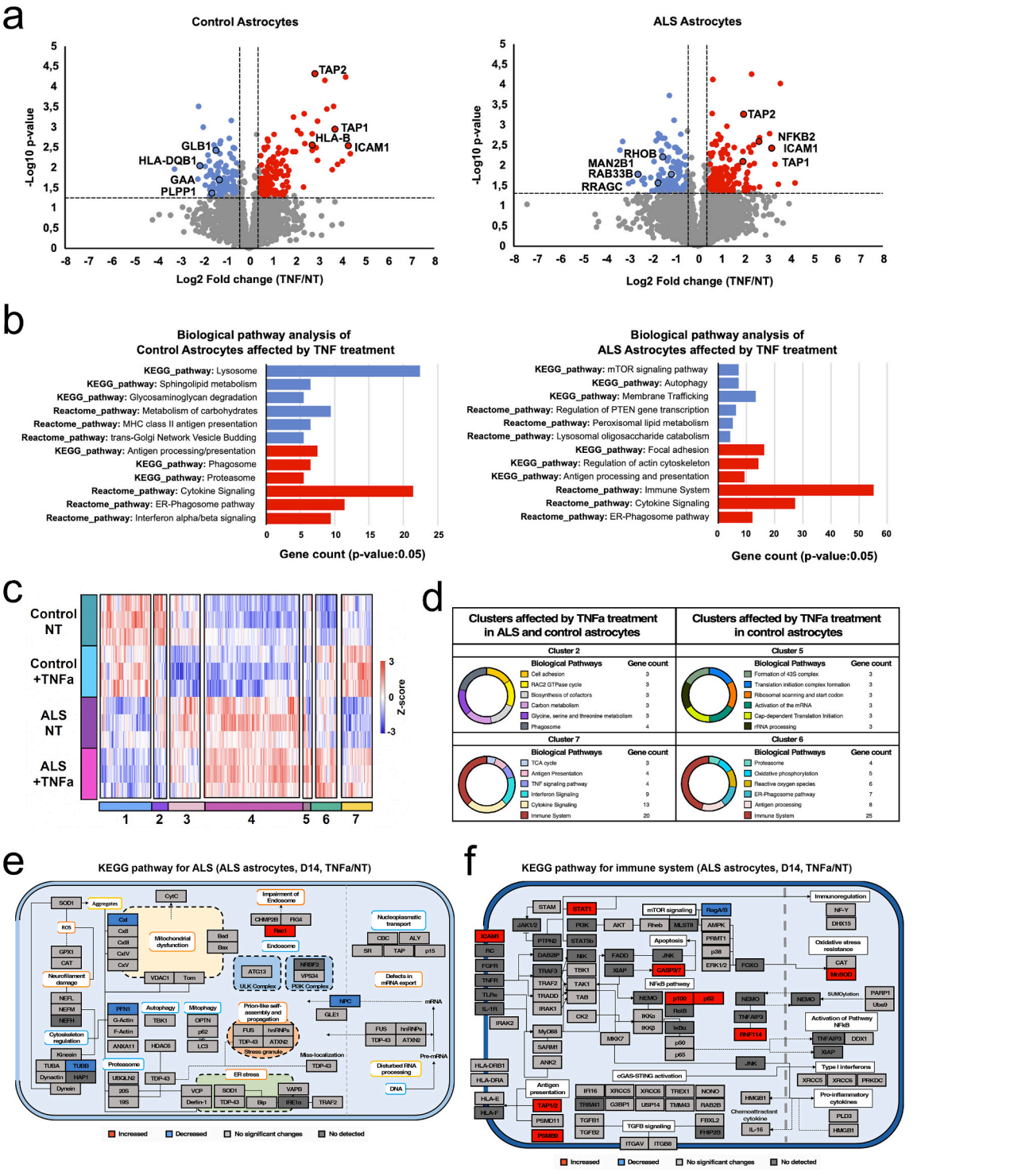

(caption on next page)

Fig. 2. a) Volcano plot of the proteome profile of control and ALS astrocytes (ALS $n = 3$, Control n = 3) at 14 days treated with tumor necrosis factor-alpha (TNF) and not treated (NT). Decreased and increased proteins are represented in blue and red, respectively (Two-tailed unpaired *t*-test *p*-value: 0.05; log2 fold-change cutoffs of +0.5).
b) Biological pathway analysis of dysregulated proteins of control and ALS astrocytes (ALS $n = 3$, Control n = 3) at 14 days treated with tumor necrosis factor-alpha (TNF) (Enrichment *p*-value <0.05). Pathways derived from decreased and increased proteins are represented in blue and red, respectively. Lysosomal and cytokine signalling are the most enriched altered pathways in the control condition. Membrane trafficking and immune system perturbations are the main alterations detected in ALS astrocytes after TNF treatment.
c) Hierarchical clustering analysis of altered protein abundances of control and ALS astrocytes (ALS $n = 3$, Control n = 3) (One-way ANOVA *p*-value: 0.05; Tukey´s HSD FDR: 0.05) using Pearson correlation distance. The abundance of the protein groups decreased and increased are represented in blue and red, respectively.
d) Charts of pathway analysis derived from protein clusters linked to the TNF response (Enrichment *p*-value <0.05).
e) ALS mapping based on KEGG mapper color analysis. Protein abundances of ALS astrocytes ($n = 3$) at 14 days after TNF treatment were considered in this representation (Two-tailed *t*-test *p*-value: 0.05; log2 fold-change cutoffs of +0.5). The ALS pathway map shows no significant changes in ALS astrocytes treated to TNF compared to ALS astrocytes not treated at 14 days.
f) Immune mapping based on KEGG mapper color and Reactome analysis. Protein abundances of ALS astrocytes (n = 3) at 14 days after TNF treatment were considered in this representation (Two-tailed unpaired *t*-test *p*-value: 0.05; log2 fold-change cutoffs of +0.5). Protein mapping highlights the increase in antigen presentation and non-canonical NF-kB pathway. (For interpretation of the references to color in this figure legend, the reader is referred to the web version of this article.)

Relative to treated or un-treated WT astrocytes, however, ALS astrocytes showed activated NF-κB and cytokine signalling pathways, and marked reduction of metabolism of RNA and proteins pathways (Fig. S2a). ALS astrocytes also had decreased mitochondrial and proteasome proteins, but increased autophagy (i.e., ATG13) and nuclear transport proteins (i.e., GLE1, NCP; Fig. S2b). A detailed analysis of the immune mapping showed that ALS astrocytes preferentially activated NF-κB through the non-canonical pathway, increasing the expression of MHC-I molecules and chemoattractant cytokines (such as IL-16; Fig. S2c). We also observed perturbations in mTOR signalling (e.g., AKT, Rheb, MLST8). Thus, ALS astrocytes reactivity is different from that of WT astrocytes treated with TNFα. These data suggest that preclinical therapy testing should be evaluated in patient cells rather than WT cells treated to phenocopy or pathocopy diseased cells.

2.3. FGF4 reverses ALS astrocyte dysfunction and reactivity

Since FGF signalling can modulate astrocyte physiology, reactivity, and excitotoxicity (Kang et al., 2014b), we evaluated the potential effect of FGF2, FGF4, FGF16, and FGF18 (Savchenko et al., 2019) in reversing the altered biological pathways in ALS astrocytes. To induce FGF overexpression, we transduced astrocytes with AAV particles encoding FGFs, and compared them to astrocytes that were transduced with a control AAV vector expressing green fluorescent protein (GFP; Fig. 3a-c). We then used proteomics to detect changes in protein profiles 14 days after astrocyte transduction (Table S2). We confirmed FGF expression in the intracellular and released fractions using proteomics and ELISA assays (Fig. 3c and Fig. S3). There were no significant differences in protein expression between non-treated (NT) and AAV-GFP-treated (GFP) astrocytes (Fig. 3d and e), indicating that GFP expression had no obvious effect on astrocyte proteomes. Hierarchical clustering analysis (One-way ANOVA, *p*-value: 0.05; Tukey´s HSD FDR: 0.05) of WT astrocytes showed two clusters (Cluster 1 and Cluster 2) that differed in which proteins decreased and increased in abundance, respectively (Fig. 3d). Cluster 1 is mainly associated with cell adhesion, extracellular matrix interaction, and RNA metabolism, while Cluster 2 is involved in vesicle transport, cytoskeleton regulation, proteasome, and amino acid metabolism (Fig. 3d). Interestingly, WT astrocytes showed minimal response to any FGF.

We also found two main clusters of dysregulated proteins in ALS astrocytes (Fig. 3e). Cluster 1 consisted of down-regulated proteins related to glutathione metabolism, phagosome, spliceosome, innate immune system, and RNA metabolism. Cluster 2 includes up-regulated proteins related to cytoskeleton regulation, vesicle transport, extracellular matrix interaction, and phosphatidylinositol signalling. In these $SOD1^{A4V}$ ALS astrocytes, FGF4 triggered profound alterations in the immune system pathway, mitochondrial function, cytoskeleton, and cGAS-STING signalling axis regulation (Fig. 3h and I, Table S2). Thus, we wondered if FGF4 was acting on the same dysregulated innate immune-related proteins we previously detected in D14 ALS astrocytes (from Fig. 1). Surprisingly, we found significant overlap between FGF4-regulated proteins and all immune system-related proteins that were altered in D14 ALS astrocytes (Fig. 3g), and for dysregulated proteins of the ALS pathway (Fig. 3f). We also found that FGF4 treatment "reversed" protein changes observed in D14 ALS astrocytes, specifically those protein clusters related to the immune system, proteasome function, and axon guidance (Cluster 3), and focal adhesion and endocytosis (Cluster 5;Fig. S4a and b). Protein clusters 2 and 4 (enriched with proteins involved in glycolipid metabolism and DNA repair, respectively) were minimally affected by FGF4 transduction. Notably, in ALS astrocytes (Fig. S4d), FGF4 distinctly and significantly changed the abundance of proteins associated with pyruvate metabolism, the cGMP-PKG pathway (Cluster 1), and processes such as glutamate signalling, membrane trafficking, and neurodegeneration (Cluster 6).

Relative to FGF4-treated WT astrocytes, FGF4-treated ALS astrocytes had reduced levels of glycolysis/gluconeogenesis, protein and glutathione metabolism, and immune system proteins (Fig. S5a). However, they showed increased abundance of proteins linked to RNA metabolism and interferon signalling (Fig. S5a left panel, e.g., YTHDF2, SAMHD1; Table S2). A more detailed examination of the ALS pathway revealed that proteins involved in apoptosis activation and mitochondrial complex I were increased in FGF4-treated ALS $SOD1^{A4V}$ astrocytes, while the abundance of proteins related to cytoskeleton regulation, proteasome, ER stress, and other components of the electron transport chain decreased. The immune mapping indicated a downregulation of proteins related to the cGAS-STING pathway (e.g., RAB2B, XRCC5, XRCC6) and mTOR signalling, including Rheb, RagA/B, and ERK1/2. Overall, the data suggested that FGF4 transduction could be a promising approach for lowering the immune response of ALS astrocytes in vivo.

2.4. FGF4 lowers ALS astrocyte reactivity in vivo but fails to protect ALS motor neurons from death

We next sought to investigate whether delivering FGF4 in vivo could reduce glial reactivity and motor neuron degeneration. We intrathecally injected $SOD1^{G93A}$ mice at 60 days of age (pre-symptomatic stage) with an AAV serotype 9 vector expressing GFP or FGF4 (Fig. 4a), with the transgenes expressed from the astrocyte-specific gfa_{ABC1D} promoter (Rochat et al., 2022; Lee et al., 2008). At D140 post-injection (symptomatic stage (Raoul et al., 2005)), we collected the spinal cords, and confirmed successful delivery and expression of the transgene using the GFP reporter vector. As expected, GFP expression was limited to astrocytes in the white and grey matter of the spinal cord (Fig. 4b-d). We measured GFAP intensity as a proxy for astrocyte reactivity (Fig. 4e and f) and found a significant increase in glial response in $SOD1^{G93A}$ mice with AAV9-gfa_{ABC1D}::GFP vector compared to WT mice. Importantly,

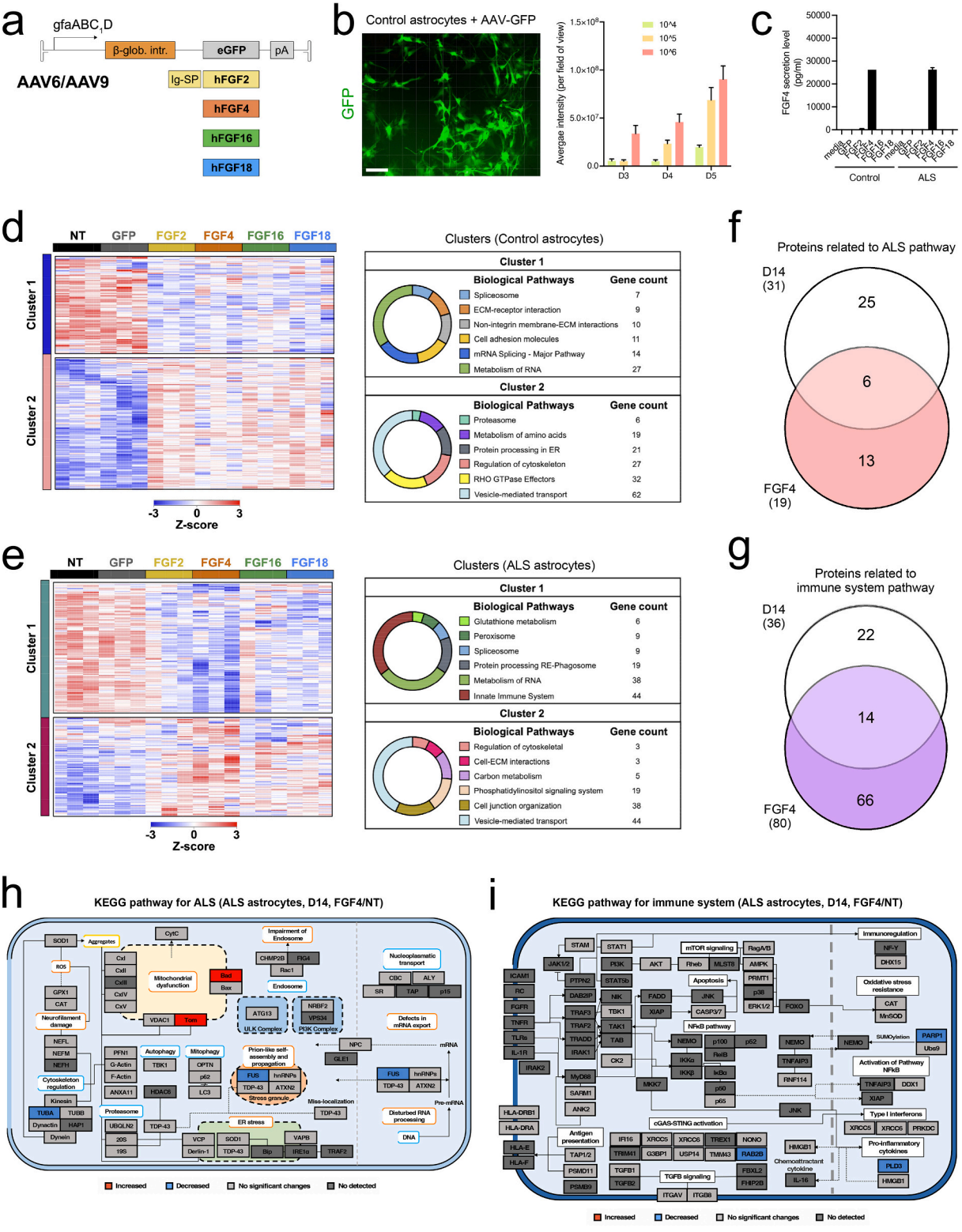

(caption on next page)

Fig. 3. a) Schematic representation of AAV vectors.
b) Astrocytes transduced with control AAV vector express GFP. Scale bar, 100 μm. The bar diagram shows levels of natural GFP in control astrocytes at 3, 4 and 5 days post-transduction with different concentrations of viruses.
c) Bar diagram shows the quantity of FGF4 release in the medium by AAV-FGF4 transduced astrocytes, measured by ELISA ($n = 2$ independent experiments with triplicate wells measured for each experiment).
d and **e)** Hierarchical clustering analysis of dysregulated proteins in control **(d)** and ALS **(e)** astrocytes (ALS n = 3, Control n = 3) treated with different FGFs (One-way ANOVA p-value: 0.05; Tukeý s HSD FDR: 0.05) using Pearson correlation distance. The abundance of the protein groups decreased and increased are represented in blue and red, respectively. Charts of pathway analysis derived from clusters 1 and 2 (Enrichment p-value <0.05) represent the protein groups changed after FGFs treatment.
f and **g)** Venn diagram of dysregulated proteins related to ALS pathways and immune system pathways detected in ALS and control astrocytes (ALS n = 3, Control n = 3) on day 14 and FGF4 treated condition.
h) ALS mapping based on KEGG mapper color analysis. Protein abundances of ALS astrocytes (n = 3) at 14 days after FGF4 treatment were considered in this representation (One-way ANOVA *p*-value: 0.05; Tukeý s HSD FDR: 0.05). The ALS pathway map reveals a significant effect of FGF4 treatment in ALS astrocytes reversing the dysregulation of the proteins associated with the mitochondrial and proteasome function.
i) Immune mapping based on KEGG mapper color and Reactome analysis. Protein abundances of ALS astrocytes (n = 3) at 14 days after FGF4 treatment were considered in this representation (One-way ANOVA *p*-value: 0.05; Tukeý s HSD FDR: 0.05). Protein mapping shows the impact of FGF4 treatment on ALS astrocytes reversing the protein changes linked to the activation of the innate immune system. (For interpretation of the references to color in this figure legend, the reader is referred to the web version of this article.)

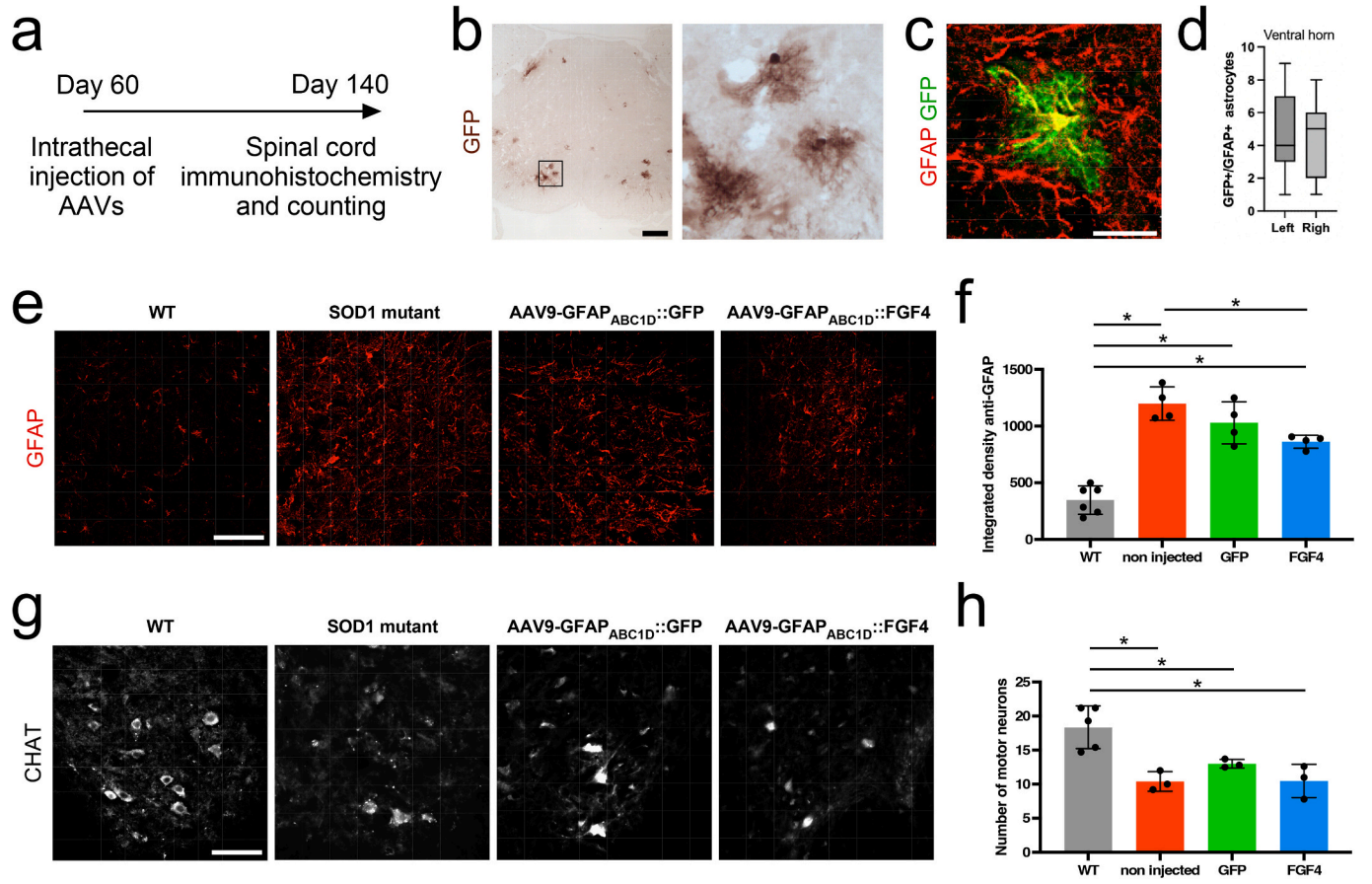

Fig. 4. a) Experimental workflow: 60-day-old SOD1G93A mice were intrathecally injected with AAVs, and the spinal cord was collected at days 90 and 140 to perform immunohistochemistry.
b) Representative image of the spinal cord stained for GFP, 30 days following intrathecal injection of AAV9-gfaABC1D-GFP. At higher magnification (right panel), GFP-positive cells show a highly complex morphology typical of astrocytes. Scale bar, 200 μm.
c) Immunostaining for GFAP (in red) and GFP (in green) cells in the spinal cord of 90-day-old SOD1 mutant mice injected with AAV9-gfaABC1D-GFP. Scale bar, 25 μm.
d) Box-and-whiskers plot of the number of GFP + GFAP+ astrocytes observed on each side of the ventral horn of the spinal cord. Mice were intrathecally injected with AAV9-gfaABC1D-GFP at day 60 and spinal collected 30 days later ($n = 4$).
e) Representative immunofluorescence staining of GFAP in the spinal cord of 140-day-old wildtype, SOD1G93A, and SOD1G93A mice injected with the indicated AAVs. Scale bar = 100 μm.
f) Bar graph of the GFAP fluorescence signal intensity in the ventral horn of the spinal cord of mice of indicated genotype, injected or not with AAV9-gfaABC1D-GFP and AAV9-gfaABC1D- FGF4. $n = 3$–5, values are mean ± SEM, $^*P < 0.05$, one-way ANOVA with Tukey's post hoc test.
g) Representative images of the ventral horn of the spinal cord immunostained for ChAT (white) from the different experimental groups. Scale bar = 100 μm.
h) Quantification of the number of ChAT+ motoneurons in the lumbar spinal cord of 140-day-old mice injected or not with AAV9-gfaABC1D-GFP and AAV9-gfaABC1D-FGF4 ($n = 3$–5). Values are mean ± SEM, $^*p < 0.05$, one-way ANOVA with Tukey's post hoc test. (For interpretation of the references to color in this figure legend, the reader is referred to the web version of this article.)

local expression of FGF4 significantly, but not completely, reduced astrocyte reactivity in $SOD1^{G93A}$ mice (Fig. 4e and f). Finally, we measured MN survival by counting the number of choline acetyltransferase (C-positive neurons in the ventral horn of the lumbar SC of $SOD1^{G93A}$ mice (Fig. 4g and h). Compared to WT mice, we observed a significant loss of MNs in non-injected $SOD1^{G93A}$ mice and those injected with AAV9-GFA_{ABC1D}::GFP. Unfortunately, FGF4 did not appear to protect MNs from cell death despite the ALS astrocytes being less reactive.

2.5. ALS astrocyte reactivity reduced by FGF4 is abrogated by TNFα

Work in vivo showed that despite lowering astrocyte reactivity in ALS, FGF4 could not prevent MNs from cell death. We hypothesized that a complete rescue of the ALS phenotype (reversing astrocyte reactivity and preventing MNs death) by FGF4, could not be achieved due to ongoing complex neuroinflammatory processes in vivo. To gain further insight, we examined how the astrocyte proteome was modulated when cells were co-treated with FGF4 and proinflammatory cytokine TNFα in vitro. Volcano plots showed a consistent increase in proteins related to antigen presentation in both control and ALS astrocytes treated with TNFα+FGF4 (Fig. 5a), along with a substantial increase in proteins associated with oxidative stress in the ALS astrocytes (e.g., SOD2). The biological pathway analysis of the control condition (Fig. 5b, left panel) indicated a decline in the proteins involved in the apoptotic process, lysosome function, and keratan sulfate degradation, accompanied by an increase in proteins related to the immune system, membrane trafficking, and mRNA surveillance. In contrast, the ALS astrocytes showed an underrepresentation of the membrane trafficking pathway, cytokine signalling, and ubiquitin-mediated proteolysis, while simultaneously exhibiting an increase in immune-related proteins and proteins involved in RNA and amino acid metabolism (Fig. 5b, right panel). These findings suggest that in response to TNFα+FGF4, ALS astrocytes could modulate some aspects of inflammation related to cytokine signalling (Fig. 5b, right panel), such as the reduction of proteins involved in interferon-gamma signalling (e.g., TRIM22; Table S2), and NF-kB activation (e.g., RELA, CUL1, TAB1; Table S2). However, they are unable to completely inhibit the activation of the immune system and ALS-related biological processes.

We next used the ALS and immune system maps to identify the specific protein changes connected to TNFα+FGF4 treatment in ALS astrocytes (Fig. 5c and d). $SOD1^{A4V}$ astrocytes increased some components of the mitochondrial respiratory complex, proteasome, and antioxidant enzymes, such as catalase and glutathione peroxidase 1 (Fig. 5c). We also observed increased protein levels involved in NEMO SUMOylation (i.e., PARP1, UBS9), innate immune response regulation, activation of the cGAS-STING pathway (e.g., XRCC5, XRCC6, NONO, RAB2B), Toll-like receptor (TLR) signalling (e.g., MYD88, PLD3), and mTOR signalling (e.g., PRMT1, ERK 1/2). TNFα+FGF4 treatment also increased proteins related to the regulation of TGFB signalling (e.g., SDCBP, AIMP1, HSP90AB1; Table S2), and important secreted factors such as macrophage migration inhibitory factor (MIF; Table S2).

Finally, we compared the responsiveness of ALS versus WT astrocytes to TNFα+FGF4 treatment (Fig. S6a-c), and found that ALS astrocytes have increased levels of proteins related to innate immunity, apoptosis regulation, and lysosomal and proteasomal function (Fig. S6a). However, there was a decrease in membrane traffic, mRNA surveillance, and cytokine pathways. SOD1 astrocytes also show slightly increased levels of proteins associated with mitochondrial dysfunction, oxidative stress, proteasome function, and mitophagy (Fig. S6b). We again observed an elevation in several proteins that act with the mTOR signalling pathway (e.g., Rag A/b, AMPK, PRMT1, p38, ERK1/2), and apoptotic proteins such as caspases 3 and 7 (Fig. S6c). Interestingly, our immune mapping revealed that ALS astrocytes treated with FGF4 and TNFα (i.e., under inflammatory conditions) were less susceptible to activating NF-κB and TGFβ signalling (e.g., TGFβ2). We also noted a decrease in proteins involved in cGAMP transport, such as LRRC8D and FGF signalling (i.e., ITGB3; Table S2). ALS astrocytes also had higher levels of proteins linked to cGAS-STING regulation of the innate immune response (e.g., NONO, RAB2B), NF-κB pathway regulators (e.g., DDX1, RNF114, TNFAIP3), TLR signalling (e.g., MYD88, PLD3), and complement regulation (including complement factor I; Table S2). We also observed changes in the levels of proteins involved in regulating inflammation and cell-intrinsic initiation of autoimmunity (e.g., TREX1).

Collectively, these data show that ALS astrocytes respond differently to TNFα insult and FGF4 transduction compared to WT astrocytes. In the presence of TNFα, FGF4 did not completely block the activation of the innate immune system, suggesting that the effect of FGF4 was diminished in the in vivo pro-inflammatory environment.

3. Discussion

Accumulated evidence suggests that neuroinflammation is a key driver of MN degeneration in ALS (Liu and Wang, 2017). Astrocytes display an inflammatory profile even in the pre-symptomatic phase of the disease, suggesting their contribution to the non-cell autonomous mechanisms underlying ALS progression. In this study, we demonstrate that ALS astrocytes undergo time-dependent protein changes linked to the progression of ALS pathology. Through proteomics analysis, we show that $SOD1^{A4V}$ astrocytes have elevated basal levels of proteins associated with mitochondrial dysfunction, nucleoplasmic transport, RNA processing, prion-like self-assembly and propagation, the proteasome, and the innate immune system.

Increased mitochondrial complexes are associated with the production of reactive oxygen species (ROS) (Zhao et al., 2019). Excess ROS can lead to the opening of the mitochondrial permeability transition pore (mPTP) (Kent et al., 2021), resulting in cytosolic escape of mitochondrial DNA (mtDNA), which in turn activates the innate immune response (Kim et al., 2023). Our data reveal an upregulation of VDAC1, one of the main proteins involved in this process (Decout et al., 2021; Kim et al., 2019a), and an increase in cytosolic DNA sensors such as XRCC5/XRCC6 (Sui et al., 2021). We also identified proteins that activate cGAS (i.e., G3BP1) (Kim et al., 2019b) and modulate STING signalling at the ER membrane (i.e., TMEM43) (Fenech et al., 2020). Our results therefore align with recent studies showing that mtDNA release activates the cGAS-STING-pathway in both TDP-43 iPSC-derived neurons in vitro (Yu et al., 2020) and TDP43 and SOD1 mutated animal models of ALS (Tan et al., 2022). We corroborated that the TNFα supply evoked an exacerbation of the immune pathways related to antigen presentation and NF-κB activation. However, TNFα alone failed to replicate the innate immune response and mitochondrial dysfunction observed in the iPSC-derived ALS astrocytes, highlighting these as unique molecular signatures of the ALS astrocyte phenotype. This evidence strongly suggests that the cGAS-STING pathway is a significant early pathogenic feature of ALS astrocytes.

FGF family members are associated with improved astrocyte functions, such as increased GLT1 expression (Savchenko et al., 2019; Roybon et al., 2013) and immunomodulation in different inflammatory diseases (Song et al., 2022). FGF4 is also downregulated in the gene expression profile of ALS SC grey matter post-mortem tissues (Dangond et al., 2004). We hypothesized that the overexpression of FGFs can reverse astrocyte dysfunction and reactivity in ALS. To test this, we engineered AAV vectors to express and release FGF2, 4, 16 or 18 as these factors increase in GLT1 levels and decrease GFAP levels in WT rodent and human astrocytes in vitro (Savchenko et al., 2019; Roybon et al., 2013). Upon transduction with FGFs, ALS astrocytes exhibited changes in proteins related to ALS pathology and the immune system, including the innate immune cGAS-STING pathway (Figs. 1 and 3). Notably, ALS astrocytes showed a stronger response to FGF4 transduction.

The biological functions of FGF4 include promoting growth (Kook et al., 2013), survival (Son et al., 2020), angiogenesis (Fukuyama et al.,

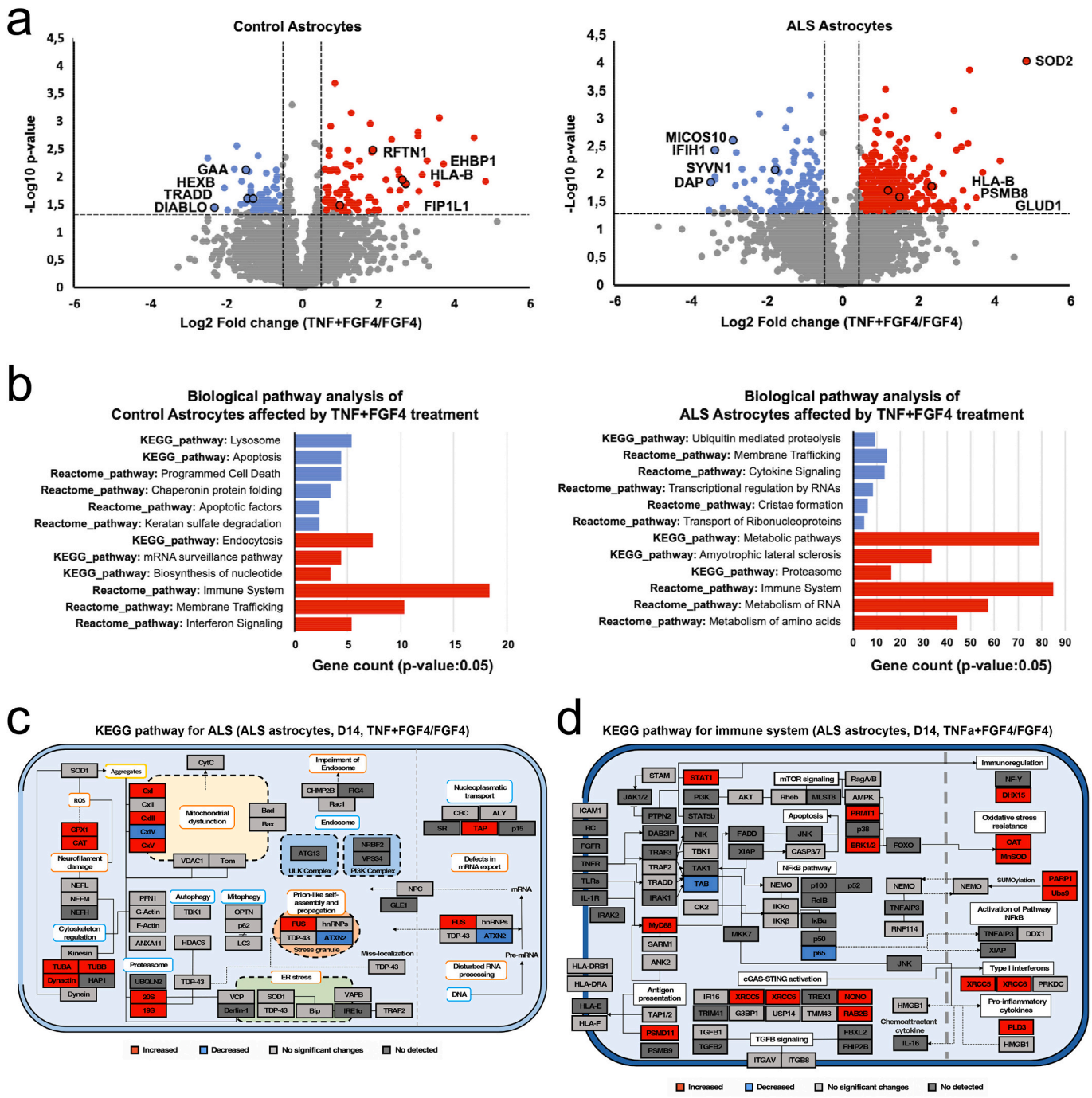

Fig. 5. a) The volcano plot shows the proteome of control and ALS astrocytes (ALS n = 3, Control n = 3) at 14 days treated with TNF + FGF4 compared to FGF4 alone. Decreased and increased proteins are represented in blue and red, respectively (Two-tailed unpaired *t*-test *p*-value: 0.05; log2 fold-change cutoffs of +0.5). **b)** Biological pathway analysis of protein changes in control and ALS astrocytes (ALS n = 3, Control n = 3) at 14 days treated with TNF + FGF4 vs. FGF4 alone (Enrichment *p*-value <0.05). The decreased and increased proteins are represented in blue and red, respectively. Lysosomal and immune system signalling are the most enriched altered pathways in the control condition. In contrast, membrane trafficking and the immune system remain the main dysregulated pathways in ALS astrocytes.

c) ALS mapping based on KEGG mapper color analysis. Protein abundances of ALS astrocytes (n = 3) at 14 days treated with TNF + FGF4 versus FGF4 were considered in this representation. The *p*-value of the two-tailed unpaired *t*-test is 0.05 with log2 fold-change cutoffs of +0.5. The data show that under a pro-inflammatory environment, the treatment with FGF4 fails in reverting the mitochondrial and proteasome dysregulated proteins.

d) Immune mapping based on KEGG mapper color and Reactome analysis. Protein abundances of ALS astrocytes (n = 3) at 14 days treated with TNF + FGF4 vs. FGF4 were considered in this representation (Two-tailed unpaired t-test p-value: 0.05; log2 fold-change cutoffs of +0.5). Protein mapping confirms that FGF4 treatment in the presence of TNF partially reduces the protein changes linked to immune system activation. (For interpretation of the references to color in this figure legend, the reader is referred to the web version of this article.)

2007), metabolism (Fan et al., 2022), and apoptosis regulation (Khromov et al., 2012). Emerging evidence suggests that FGF4 also modulates the immune system in early life stages (van Bilsen et al., 2020). FGF signalling can regulate and interact with various pathways, including Ras/Raf-MEK-MAPKs and PI3K/AKT/mTOR (Xie et al., 2020). Our findings indicate that FGF4 mitigates some protein profile changes linked to ALS and innate immune system pathways in $SOD1^{A4V}$ astrocytes in vitro, particularly affecting components of the cGAS-STING pathway and reducing proteins associated with mTOR signalling. FGF signalling can either activate (Pei et al., 2023) or inhibit (Su et al., 2020) the mTOR pathway depending on the context. Interestingly, mTOR pathway inhibition suppresses STING in vitro when monocytes derived from lupus erythematosus patients are treated with rapamycin (Murayama et al., 2020). The exact mechanisms by which FGF4 modulates innate immunity in pathological astrocytes require further investigation.

Despite the ability of FGF4 to significantly reduce astrocyte reactivity, it did not improve MN survival in vivo. We, therefore, investigated the molecular changes induced by FGF4 transduction in ALS and control astrocytes under a pro-inflammatory environment in vitro. Proteomic analysis revealed that ALS astrocytes maintained high levels of proteins related to the cGAS-STING pathway, such as XRCC5/XRCC6, and scaffold elements for IRF3 phosphorylation (e.g., NONO, RAB2B) (Morchikh et al., 2017; Takahama et al., 2017). Previous studies have shown that complete blockage of the cGAS-STING pathway is necessary to ameliorate ALS progression and survival in vivo *(Yu et al., 2020; Tan et al., 2022)*. Interestingly, $SOD1^{A4V}$ astrocytes treated with TNFa+FGF4 showed a significant increase in proteins linked to the mTOR and the cGAS-STING pathways. The activation of mTOR signalling, and downstream members of the TLR and interleukin-1 receptor families, such as MYD88, are crucial for metabolic remodelling during the immune response (Bai and Liu, 2019; Powell et al., 2012; Deguine and Barton, 2014). Similarly, ALS astrocytes treated with TNFα+FGF4 exhibited high levels of MIF, a pro-inflammatory cytokine associated with chronic neuroinflammation and neurodegeneration (Nasiri et al., 2020; Zhang et al., 2023). We also observed a decline in proteins such as the LRRC8D subunit, which is associated with increased cGAMP transport to neighboring cells (Lahey et al., 2020), and a reduction in the secreted complement factor I, a regulator of complement activation (Altmann et al., 2020; Xue et al., 2017). Our data further indicated that ALS astrocytes treated with TNFα+FGF4 experienced disruptions in the TGFβ signalling pathway, previously linked to ALS progression (Galbiati et al., 2020). Reduced levels of TGFβ-2 have been associated with synaptic dysfunction (Heupel et al., 2008), and high dose of TGFβ-2 have been shown to transiently improve motor performance in SOD1 mutant mice (Day et al., 2005).

Our findings suggest that FGF4 treatment in ALS astrocytes reduces proteins involved in mitochondrial dysfunction, RNA processing, proteosome, prion-like self-assembly and propagation, and innate immune system in vitro. Despite human and mouse SOD1 astrocytes displaying similar proinflammatory profiles (Ziff et al., 2022), delivering FGF4 to SOD1 mice does not protect MNs from cell death in vivo. This outcome is likely due to the complex neuroinflammatory mechanisms at play, involving intricate crosstalk between astrocytes and other cell types, such as microglia (Calafatti et al., 2023). It is well known that astrocytes reactivity can be induced by activated microglia, which may further compromise neuronal survival (Liddelow et al., 2017). Future studies should focus on elucidating these complex interactions and exploring combination therapies to reduce neuroinflammation and enhance neuronal survival, potentially leading to more effective treatments for ALS.

In conclusion, this study highlighted the potential of patient-derived iPSC models to capture the cell-autonomous contribution of astrocytes in ALS pathogenesis and to test new therapeutic approaches aimed at modulating astrocyte responsiveness in ALS.

4. Experimental procedures

All materials were purchased from Thermo Fisher Scientific, unless specified

4.1. Ethics

All in vitro and in vivo procedures were conducted in accordance with national and European Union directives. All animal experiments were approved by the French ministry of higher education, research and innovation (APAFIS #6224–2,016,072,711,103,977), and were conducted in compliance with the European Community and national directives for the care and use of laboratory animals.

4.2. Human iPSC Lines

Human IPSC lines were obtained from RUCDR Infinite Biologics, where the iPSCs were generated by reprogramming of ALS patient and healthy control fibroblasts with Sendai or retroviral vectors and characterized for expression of common pluripotency markers and ability to differentiate into the three germ layers. A total of 3 ALS patients and 2 control individuals were included in this study (Table S4). To obtain 3 biological replicates per group, one of the control lines was used at two different passages to initiate differentiation, as passage number affects differentiation outcomes (Cantor et al., 2022). All obtained iPSC lines had normal karyotype. The iPSCs were further expanded and biobanked. The generation of iPSC line CSC-37 N was previously published (Xue et al., 2017).

4.3. Generation of spinal cord astrocytes

The iPSCs lines were differentiated to SC astrocytes using the modified protocol originally developed by Roybon et al. (Roybon et al., 2013). Control line FA11 underwent two independent differentiations; other lines underwent one differentiation. All lines were differentiated side-by-side. Human iPSC colonies were harvested and plated to ultra-low attachment flasks (Corning) in WiCell media supplemented with 20 μM of ROCK inhibitor Y27632 (Selleck Chemicals, Munich, Germany) and 20 ng/mL of FGF2 (Peprotech). Next day, the media was replaced by WiCell media supplemented with 0.1 μM LDN193189 (Stemgent), 10 μM SB431542 (Sigma-Aldrich), and 1 μM retinoic acid (RA; Sigma-Aldrich). On D4, 50 % of WiCell media were replaced with medium composed of advanced DMEM/F12, 2 mM L-glutamine, 1 % NEAA (*v*/v), 2 % B27 Supplement without vitamin A (v/v), 1 % penicillin-streptomycin (v/v), heparin, plus LDN193189, SB431542 and RA. On D6 1 μM RA, 1 μM SAG (Selleck Chemicals), 10 ng/mL BDNF (Peprotech) and 0,4 μg/mL ascorbic acid (Sigma-Aldrich) were added to the mix of 50 % WiCell/ 50 % advanced DMEM/F12 media, at D8 and D10 to advanced DMEM/F12 and at D12-D30 to the mix of 50 % advanced DMEM/F12/50 % Neurobasal media with medium change every other day. In addition, on D12–30, 20 ng/mL GDNF (Peprotech) was added to the media. From D30 onwards, the free-floating spheres were grown in media composed of advanced DMEM/F12, 2 mM L-glutamine, 1 % NEAA (v/v), 2 % B27 supplement without vitamin A (v/v), 1 % penicillin-streptomycin (v/v) and heparin in the presence of 20 ng/mL FGF2 (Peprotech) and 20 ng/mL EGF (Peprotech). On D60, free-floating spheres were collected, washed, dissociated using accutase (Invitrogen) and single cells seeded and grown as adherent cultures in flasks coated with 100 μg/mL Poly-L-ornithine (Sigma-Aldrich) and 5 μg/mL mouse laminin in media composed of advanced DMEM/F12, 2 mM L-glutamine, 1 % NEAA (v/v), 2 % B27 supplement without vitamin A (v/v), 1 % penicillin-streptomycin (v/v), heparin and 20 ng/mL CNTF (Peprotech). From day 85, astrocytes were cultured in neural differentiation medium composed of neurobasal media, 2 mM L-glutamine, 1 % NEAA (v/v), 1 % N2 Supplement (v/v), 1 % penicillin-streptomycin (v/v), and 20 ng/mL CNTF.

4.4. Viral production and transduction

FGF-encoding constructs were generated by replacing, using standard cloning procedures, the GFP-coding sequence with cDNAs encoding the human forms of FGF4 (NM_002007.4), FGF16 (NM_003868.3) and FGF18 (NM_003862.3) in the pAAV-gfa$_{ABC1D}$-β-globin intron-GFP vector (Dirren et al., 2014). To enhance FGF2 secretion, the vector was adapted for N-terminal fusion of the protein to the immunoglobulin signal peptide, as previously described (Rinsch et al., 2001). For transgene expression in astrocytes in vivo, each of these constructs was packaged into serotype-9 AAV particles. To transduce iPSC-derived astrocytes, the same constructs were packaged into serotype-6 AAV. Briefly, for packaging into AAV vectors, HEKExpress® cells maintained in suspension were transiently transfected with pAAV and either the pDP6 and pDP9 helper plasmid. To recover released AAV particles, the cell supernatant was collected at day 3 and day 7 after transfection. At day 7, the packaging cells were lysed using repeated freeze-thawing. For purification and concentration, AAV particles were captured by affinity chromatography using POROS™ CaptureSelect™ resins (AAV9 and AAVX, Thermo Fisher Scientific, MA). AAV suspension was concentrated using centrifugal devices (Amicon® Ultra-15,100 kDa centrifugal filter devices, Merck) and resuspended in PBS with 0.001 % Pluronic-F68 before storage. The vectors were tittered by dPCR (QIAcuity® digital PCR system, QIAGEN) using an amplicon located in the β-globin intron. Overall, the method of AAV vector production was adapted from the previously described protocol (Blessing et al., 2019). To overexpress FGFs in human astrocytes, astrocytes aged days 98–107 were seeded on the plate coated with 100 μg/mL poly-L-ornithine and 5 μg/mL mouse laminin. After 3 h, the astrocytes were transduced with AAV6-GFAP-FGF2, -FGF4, -FGF16 or -FGF18 at 2 × 10(5) VG/cell. At D5 or D14 post-transduction, the cells were collected, washed with PBS and frozen at −80 °C for further analysis.

4.5. TNFα treatment

Astrocytes aged days 98–107 were seeded in 24 well plate coated with 100 μg/mL P/O and 5 μg/mL mouse laminin at the density of 120,000 cells/well. 48 h after, the cells were treated with either 100 ng/mL TNFα, or 100 ng/mL TNFα and AAV vector expressing FGF4 for 14 days. After that, the cells were washed with PBS and frozen at −80 °C until analyzed.

4.6. Immunocytochemistry and image analysis

For immunostaining, cultures were fixed using 4 % paraformaldehyde for 20 min at room temperature and non-specific binding was blocked with 10 % normal donkey serum and 0.1 % Triton X-100 in PBS for 1 h. The cells were then incubated with primary antibody to GFAP (1:1000, #Z0334, DAKO), S100b (1:500, #S2532, Sigma-Aldrich), ezrin (1:500, #3145S, Cell Signalling), GS (1:500, #MAB-302, Millipore) and ID3 (1:500, #9837S, Cell Signalling) overnight at 4 °C. The next day the cells were washed and incubated with Alexa Fluor 488 nm- (1:400; #A-21202, Molecular Probes) or 555 nm-conjugated secondary antibodies (1:400; #A-31570, Thermo Fisher Scientific) for 1 h. In addition, the cells were counterstained with DAPI (1:10,000, Life Technologies). All images were obtained using an inverted epifluorescence microscope (LRI – Olympus IX-73). Automated quantitative image analysis of stained cultures was performed with the MetaMorph Software V7.6 (Molecular Devices) using the Multi-Wavelength Cell Scoring and the Neurite Outgrowth applications. Positive cells for a specific marker were identified by their signal intensity exceeding the selected threshold. Intensity thresholds were set blinded to sample identity. For each staining, five images, each representing a different field of view per cell culture well per cell line, were analyzed. GraphPad Prism 7 software was used for statistical analysis. Data are presented as mean ± S.E.M. Unpaired two-tailed *t*-test was used to compare two groups. A *P*-value of <0.05 was considered significant. For GFAP staining intensity measurement, a log-normal generalized linear mixed-effects model with random intercepts for each replicate was used to determine if ALS measures differed from controls. Based on this analysis, ALS samples were on average, 3.9-fold higher than controls (95 % CI = 1.2–12.9; $p = 0.027$).

4.7. Enzyme-linked immunosorbent assay (ELISA)

The FGFs secretion in culture media was measured by ELISA D5 post-transduction of the cultures according to the manufacturer's instructions; FGF2, FGF4, FGF16 (all three from Thermo Fisher Scientific), FGF18 (LSBio, Seattle, WA, USA). Absorbance was measured at 450 nm.

4.8. Protein extraction and sample digestion

Proteins from astrocytes at days 5 and 14 were extracted using a lysis buffer of 25 mM DTT, 10 *w/v*% SDS in 100 mM triethylammonium bicarbonate (TEAB). The cells were sonicated using 40 cycles of 15 s on/off at 4 °C in the Bioruptor plus (model UCD-300, Diagenode). Further, the samples were boiled at 99 °C for 5 min and centrifuged at 20,000*g* for 15 min at 18 °C. The supernatants were collected to determine the protein amounts (Pierce 660 nm Protein Assay with Ionic Detergent Compatibility Reagent). Proteins were preserved at −80 °C until further use. The proteins were digested using S-Trap™ 96-well plate following the instructions of the manufacturer (ProtiFi S-Trap™ 96-well plate digestion protocol). Briefly, samples were alkylated with 50 mM IAA for 30 min in the dark at room temperature, followed by tryptic digestion in 50 mM TEAB (enzyme: substrate,1:50) at 37 °C overnight. The peptides were eluted in three steps, first with 80 μL of 50 mM TEAB, then with 80 μL of 0.2 % formic acid (FA), and finally with 80 μL of 50 % acetonitrile (ACN) containing 0.2 % FA. Peptides were dried in a speed-vac and resuspended in 0.1 % trifluoroacetic acid (TFA)/2 % ACN for peptide concentration measurement (Pierce Quantitative Colorimetric Peptide Assay).

4.9. nanoLC-MS/MS analysis and Database search

The nLC-MS/MS analysis was performed on a QExactive HF-X mass spectrometer coupled to a Dionex Ultimate 3000 RSLC nano UPLC system (Thermo Scientific), with an EASY-Spray ion source. 500 ng of peptides was analyzed from each sample using high-resolution data independent acquisition (HR-DIA). All samples were loaded onto an Acclaim PepMap 100 C18 (75 μm × 2 cm, 3 μm, 100 Å, nanoViper) trap column and separated on an Acclaim PepMap RSLC C18 column (75 μm × 50 cm, 2 μm, 100 Å)(Thermo Scientific) using a flow rate of 300 nL/min, a column temperature of 60 °C. A 110 min gradient was applied for separation, using solvents A (0.1 % formic acid) and B (0.1 % formic acid in 80 % ACN), increasing solvent B from 2 to 45 % in 95 min and to 95 % in the next 15 min, continuing for another 5 min. In HR-DIA analysis, a complete acquisition cycle consisted of 3 MS1 full scans, each followed by 18 MS2 DIA scans with variable isolation windows. Full MS1 scans were acquired using a mass range of 375–1455 *m/z*, with a resolution of 120,000 (at 200 m/z), target AGC value of 3×10^6 and maximum injection time of 50 ms. MS2 scans were acquired with a resolution of 30,000 (at 200 m/z), target AGC value of 1×10^6, automatic maximum injection time, fixed first mass of 200 m/z, NCE of 28. The variable isolation windows were 13, 16, 26 and 61 m/z with 27, 13, 8, 6 loop counts, respectively. Direct DIA analysis of the raw files was performed in Spectronaut v14 (Biognosys) against the reviewed Uniprot *Homo sapiens* sequence database (May 2022, 42,363 entries) using BGS factory default settings. The identifications were filtered by a Q value of <0.01 (equals a FDR of 1 % on peptide level). Quantification was done on MS1 level, using the top3 method.

4.10. AAV injection in mutant SOD1 mice model of ALS and power calculation

B6.Cg-Tg(SOD1*G93A)1Gur/J (*SOD1^{G93A}*) mice were purchased from the Jackson Laboratory and maintained on a C57BL/6 background. Each vector was injected at a titer of 3.10^{14} vg/mL. A volume of 10 μL of viral vectors mixed with 5 μL of lidocaine (10 mg/mL) was slowly injected between the L5 and L6 vertebraes. Appropriate injection into the intrathecal space was confirmed by the animal's tail movement and by the transiently anesthetized lower limbs. Given the significant effect of FGF4 observed in vitro and the fact that only animals successfully receiving the intrathecal injection were included in the analysis, with a large effect size between groups (Cohen's d = 0.9), we calculated that a sample size of 16 (4 animals per group) would yield a statistical test power of 0.7 at a significance level of 0.05 for the 4 groups analyzed.

4.11. Immunohistochemistry

Mice were euthanized at 140 days of age by intra-peritoneal injection of ketamine and xylazine. The mice were then transcardially perfused with PBS and the SC was incubated in 4 % paraformaldehyde in PBS for 45 min at +4 °C. After incubation, the SC was transferred to a 30 % sucrose solution and imbedded in Tissue-Tek OCT compound (Sakura Finetek). For immunofluorescence labeling, cryosections of the lumbar SC (16 μm) were collected onto Superfrost Plus glass slides. The sections were then incubated in PBS containing 0.05 % Tween-20, 0.3 % Triton-X100 and 20 % heat-inactivated donkey serum (blocking solution) for 1 h at room temperature (RT). Next, sections were incubated for 24 h at +4 °C with primary antibodies (goat anti-Chat (1:200, Merck, AB144P), mouse anti-GFAP (1:300, Merck, MAB360), and chicken anti-GFP (1:700, Abcam, Ab13970) diluted in the blocking solution. Sections were washed with PBS and incubated with fluorochrome-conjugated secondary antibodies diluted in the blocking solution for 1 h at RT. Sections were washed with PBS and mounted onto glass slides using NeoMount Fluo (NeoBiotech) solution. For chromogenic immunostaining, cryosections were incubated in Tris-buffered saline (TBS) containing 0.3 % Triton-X100 and 1.5 % donkey serum (blocking solution) for 1 h at RT. The samples were then incubated overnight at +4 °C with the primary antibody (rabbit anti-GFP, 1:600, Chromotek) diluted in the blocking solution. Sections were washed with TBS and incubated with biotinylated secondary antibody (1:100; Vector labs) diluted in blocking solution for 1 h at RT. Following several washes with 0.05 % Tween-20 in TBS, the tissue was incubated with ABC complex (Vectastain ABC kit, Vector labs kit) in 0.05 % Tween-20 in PBS for 1 h. After washing with 0.05 % Tween-20 in TBS and TB, sections were incubated with the 3,3′ diaminobenzidine substrate solution according to the manufacturer's instructions. Image acquisitions were performed using a Zeiss Axio imager microscope. For astrocytic activation, image acquisition was done on a Zeiss LSM880 Airyscan confocal microscope. The GFAP signal intensity was determined with ImageJ (National Institutes of Health).

4.12. Statistical and biological pathway analyses

Protein abundances were normalized by median subtraction following log2 transformation. Principal component and statistical analyses were performed using the Perseus 1.6.5.0 software. To compare only two conditions, the two-tailed *t*-test (*p*-value:0.05) with a cutoff of log2 ± 0.5-fold-change was applied. One-way ANOVA (p-value:0.05) and Tukey's HSD (FDR: 0.05) were done for multiple comparisons. To perform the sparse Partial Least Squares Discriminant Analysis (sPLS-DA), we used the Mixomics R package (Rohart et al., 2017) selecting the top 5 proteins in each component ($n = 3$ components). The hierarchical clustering analysis was performed using Pearson's correlation distance. The Functional Annotation Tool DAVID Bioinformatics Resources was used to detect the relevant biological pathways, considering Reactome Gene Sets and KEGG Pathway (*p*-value: 0.05).

Supplementary data to this article can be found online at https://doi.org/10.1016/j.nbd.2024.106687.

Ethical approval and consent to participate

All animal experiments were approved by the national ethics committee on animal experimentation, and were done in compliance with the European community and national directives for the care and use of laboratory animals.

Consent for publication

Not applicable.

Funding

We acknowledge funding support from the strategic research area MultiPark at Lund University. This work was supported by The French Muscular Dystrophy Association (*AFM-Téléthon*), The Crafoord Foundation, The Åhlens Foundation, and The Olle Engkvist Byggmästare Foundation. E.V. was supported by The Olle Engkvist Byggmästare Foundation, E.S. was supported by The French Muscular Dystrophy Association (*AFM-Téléthon*). S.M-M-A. is supported by the Foundation for Medical Research (FRM).

CRediT authorship contribution statement

Erika Velasquez: Writing – original draft, Validation, Methodology, Investigation, Formal analysis. **Ekaterina Savchenko:** Methodology, Investigation, Formal analysis. **Sara Marmolejo-Martínez-Artesero:** Methodology, Investigation, Formal analysis. **Désiré Challuau:** Methodology, Investigation. **Aline Aebi:** Methodology, Investigation. **Yuriy Pomeshchik:** Methodology, Investigation. **Nuno Jorge Lamas:** Writing – review & editing, Funding acquisition, Conceptualization. **Mauno Vihinen:** Writing – review & editing, Funding acquisition, Conceptualization. **Melinda Rezeli:** Writing – review & editing, Methodology, Investigation. **Bernard Schneider:** Writing – review & editing, Methodology, Funding acquisition, Conceptualization. **Cedric Raoul:** Writing – review & editing, Funding acquisition, Conceptualization. **Laurent Roybon:** Writing – review & editing, Supervision, Funding acquisition, Conceptualization.

Declaration of competing interest

The authors declare that they have no conflict of interest.

Data availability

The mass spectrometry proteomics data have been deposited to the ProteomeXchange Consortium via the PRIDE (Perez-Riverol et al., 2022) partner repository with the dataset identifier PXD045267.

Acknowledgments

We are particularly thankful to Target ALS and RUCDR Infinite Biologics (formerly Rutgers University Cell and DNA Repository) for providing the control and ALS patient iPSC cell lines. We gratefully acknowledge the support of BioMS (Swedish National Infrastructure for Biological Mass Spectrometry), and thank Zach Madaj and the Van Andel Institute (VAI)'s Bioinformatics and Biostatistics Core – Grand Rapids, MI for statistical guidance, and Dr. Darrell Chandler at the VAI for editing the manuscript.

References

Almad, A.A., Taga, A., Joseph, J., Gross, S.K., Welsh, C., Patankar, A., Richard, J.P., Rust, K., Pokharel, A., Plott, C., Lillo, M., Dastgheyb, R., Eggan, K., Haughey, N., Contreras, J.E., Maragakis, N.J., 2022. Cx43 hemichannels contribute to astrocyte-mediated toxicity in sporadic and familial ALS. Proc. Natl. Acad. Sci. USA 119 (13), e2107391119.

Altmann, T., Torvell, M., Owens, S., Mitra, D., Sheerin, N.S., Morgan, B.P., Kavanagh, D., Forsyth, R., 2020. Complement factor I deficiency: a potentially treatable cause of fulminant cerebral inflammation. Neurol Neuroimmunol Neuroinflamm 7 (3).

Bai, J., Liu, F., 2019. The cGAS-cGAMP-STING pathway: a molecular link between immunity and metabolism. Diabetes 68 (6), 1099–1108.

Bampton, A., Gittings, L.M., Fratta, P., Lashley, T., Gatt, A., 2020. The role of hnRNPs in frontotemporal dementia and amyotrophic lateral sclerosis. Acta Neuropathol. 140 (5), 599–623.

Blasco, H., Mavel, S., Corcia, P., Gordon, P.H., 2014. The glutamate hypothesis in ALS: pathophysiology and drug development. Curr. Med. Chem. 21 (31), 3551–3575.

Blessing, D., Vachey, G., Pythoud, C., Rey, M., Padrun, V., Wurm, F.M., Schneider, B.L., Deglon, N., 2019. Scalable production of AAV vectors in Orbitally shaken HEK293 cells. Mol Ther Methods Clin Dev 13, 14–26.

Calafatti, M., Cocozza, G., Limatola, C., Garofalo, S., 2023. Microglial crosstalk with astrocytes and immune cells in amyotrophic lateral sclerosis. Front. Immunol. 14, 1223096.

Cantor, E.L., Shen, F., Jiang, G., Tan, Z., Cunningham, G.M., Wu, X., Philips, S., Schneider, B.P., 2022. Passage number affects differentiation of sensory neurons from human induced pluripotent stem cells. Sci. Rep. 12 (1), 15869.

Dangond, F., Hwang, D., Camelo, S., Pasinelli, P., Frosch, M.P., Stephanopoulos, G., Stephanopoulos, G., Brown Jr., R.H., Gullans, S.R., 2004. Molecular signature of late-stage human ALS revealed by expression profiling of postmortem spinal cord gray matter. Physiol. Genomics 16 (2), 229–239.

Day, W.A., Koishi, K., Nukuda, H., McLennan, I.S., 2005. Transforming growth factor-beta 2 causes an acute improvement in the motor performance of transgenic ALS mice. Neurobiol. Dis. 19 (1–2), 323–330.

Decout, A., Katz, J.D., Venkatraman, S., Ablasser, A., 2021. The cGAS-STING pathway as a therapeutic target in inflammatory diseases. Nat. Rev. Immunol. 21 (9), 548–569.

Deguine, J., Barton, G.M., 2014. MyD88: a central player in innate immune signaling. F1000Prime Rep 6, 97.

Di Giorgio, F.P., Carrasco, M.A., Siao, M.C., Maniatis, T., Eggan, K., 2007. Non-cell autonomous effect of glia on motor neurons in an embryonic stem cell-based ALS model. Nat. Neurosci. 10 (5), 608–614.

Dirren, E., Towne, C.L., Setola, V., Redmond Jr., D.E., Schneider, B.L., Aebischer, P., 2014. Intracerebroventricular injection of adeno-associated virus 6 and 9 vectors for cell type-specific transgene expression in the spinal cord. Hum. Gene Ther. 25 (2), 109–120.

Fan, M., Pan, T., Jin, W., Sun, J., Zhang, S., Du, Y., Chen, X., Chen, Q., Xu, W., Choo, S. W., Zhu, G., Chen, Y., Zhou, J., 2022. FGF4, A new potential regulator in gestational diabetes mellitus. Front. Pharmacol. 13, 827617.

Fang, T., Al Khleifat, A., Meurgey, J.H., Jones, A., Leigh, P.N., Bensimon, G., Al-Chalabi, A., 2018. Stage at which riluzole treatment prolongs survival in patients with amyotrophic lateral sclerosis: a retrospective analysis of data from a dose-ranging study. Lancet Neurol. 17 (5), 416–422.

Fenech, E.J., Lari, F., Charles, P.D., Fischer, R., Laetitia-Thezenas, M., Bagola, K., Paton, A.W., Paton, J.C., Gyrd-Hansen, M., Kessler, B.M., Christianson, J.C., 2020. Interaction mapping of endoplasmic reticulum ubiquitin ligases identifies modulators of innate immune signalling. Elife 9.

Fukuyama, N., Tanaka, E., Tabata, Y., Fujikura, H., Hagihara, M., Sakamoto, H., Ando, K., Nakazawa, H., Mori, H., 2007. Intravenous injection of phagocytes transfected ex vivo with FGF4 DNA/biodegradable gelatin complex promotes angiogenesis in a rat myocardial ischemia/reperfusion injury model. Basic Res. Cardiol. 102 (3), 209–216.

Galbiati, M., Crippa, V., Rusmini, P., Cristofani, R., Messi, E., Piccolella, M., Tedesco, B., Ferrari, V., Casarotto, E., Chierichetti, M., Poletti, A., 2020. Multiple roles of transforming growth factor Beta in amyotrophic lateral sclerosis. Int. J. Mol. Sci. 21 (12).

Guidotti, G., Scarlata, C., Brambilla, L., Rossi, D., 2021. Tumor necrosis factor alpha in amyotrophic lateral sclerosis: friend or foe? Cells 10 (3).

Heupel, K., Sargsyan, V., Plomp, J.J., Rickmann, M., Varoqueaux, F., Zhang, W., Krieglstein, K., 2008. Loss of transforming growth factor-beta 2 leads to impairment of central synapse function. Neural Dev. 3, 25.

Juneja, T., Pericak-Vance, M.A., Laing, N.G., Dave, S., Siddique, T., 1997. Prognosis in familial amyotrophic lateral sclerosis: progression and survival in patients with glu100gly and ala4val mutations in cu, Zn superoxide dismutase. Neurology 48 (1), 55–57.

Kang, W., Balordi, F., Su, N., Chen, L., Fishell, G., Hebert, J.M., 2014a. Astrocyte activation is suppressed in both normal and injured brain by FGF signaling. Proc. Natl. Acad. Sci. USA 111 (29), E2987–E2995.

Kang, K., Lee, S.W., Han, J.E., Choi, J.W., Song, M.R., 2014b. The complex morphology of reactive astrocytes controlled by fibroblast growth factor signaling. Glia 62 (8), 1328–1344.

Kawahara, Y., Kwak, S., Sun, H., Ito, K., Hashida, H., Aizawa, H., Jeong, S.Y., Kanazawa, I., 2003. Human spinal motoneurons express low relative abundance of GluR2 mRNA: an implication for excitotoxicity in ALS. J. Neurochem. 85 (3), 680–689.

Kent, A.C., El Baradie, K.B.Y., Hamrick, M.W., 2021. Targeting the mitochondrial permeability transition pore to prevent age-associated cell damage and neurodegeneration. Oxidative Med. Cell. Longev. 2021, 6626484.

Khromov, T., Dressel, R., Siamishi, I., Nolte, J., Opitz, L., Engel, W., Pantakani, D.V., 2012. Apoptosis-related gene expression profiles of mouse ESCs and maGSCs: role of Fgf4 and Mnda in pluripotent cell responses to genotoxicity. PLoS One 7 (11), e48869.

Kiernan, M.C., Vucic, S., Cheah, B.C., Turner, M.R., Eisen, A., Hardiman, O., Burrell, J.R., Zoing, M.C., 2011. Amyotrophic lateral sclerosis. Lancet 377 (9769), 942–955.

Kim, C., 2015. iPSC technology–Powerful hand for disease modeling and therapeutic screen. BMB Rep. 48 (5), 256–265.

Kim, J., Gupta, R., Blanco, L.P., Yang, S., Shteinfer-Kuzmine, A., Wang, K., Zhu, J., Yoon, H.E., Wang, X., Kerkhofs, M., Kang, H., Brown, A.L., Park, S.J., Xu, X., Zandee van Rilland, E., Kim, M.K., Cohen, J.I., Kaplan, M.J., Shoshan-Barmatz, V., Chung, J. H., 2019a. VDAC oligomers form mitochondrial pores to release mtDNA fragments and promote lupus-like disease. Science 366 (6472), 1531–1536.

Kim, S.S., Sze, L., Liu, C., Lam, K.P., 2019b. The stress granule protein G3BP1 binds viral dsRNA and RIG-I to enhance interferon-beta response. J. Biol. Chem. 294 (16), 6430–6438.

Kim, J., Kim, H.S., Chung, J.H., 2023. Molecular mechanisms of mitochondrial DNA release and activation of the cGAS-STING pathway. Exp. Mol. Med. 55 (3), 510–519.

Kook, S.H., Jeon, Y.M., Lim, S.S., Jang, M.J., Cho, E.S., Lee, S.Y., Choi, K.C., Kim, J.G., Lee, J.C., 2013. Fibroblast growth factor-4 enhances proliferation of mouse embryonic stem cells via activation of c-Jun signaling. PLoS One 8 (8), e71641.

Kwiatkowski Jr., T.J., Bosco, D.A., Leclerc, A.L., Tamrazian, E., Vanderburg, C.R., Russ, C., Davis, A., Gilchrist, J., Kasarskis, E.J., Munsat, T., Valdmanis, P., Rouleau, G.A., Hosler, B.A., Cortelli, P., de Jong, P.J., Yoshinaga, Y., Haines, J.L., Pericak-Vance, M.A., Yan, J., Ticozzi, N., Siddique, T., McKenna-Yasek, D., Sapp, P. C., Horvitz, H.R., Landers, J.E., Brown Jr., R.H., 2009. Mutations in the FUS/TLS gene on chromosome 16 cause familial amyotrophic lateral sclerosis. Science 323 (5918), 1205–1208.

Lahey, L.J., Mardjuki, R.E., Wen, X., Hess, G.T., Ritchie, C., Carozza, J.A., Bohnert, V., Maduke, M., Bassik, M.C., Li, L., 2020. LRRC8A:C/E Heteromeric channels are ubiquitous transporters of cGAMP. Mol. Cell 80 (4), 578–591 e5.

Lamas, N.J., Roybon, L., 2021. Harnessing the potential of human pluripotent stem cell-derived motor neurons for drug discovery in amyotrophic lateral sclerosis: from the clinic to the laboratory and Back to the patient. Frontiers in Drug Discovery 1.

Larson, T.C., Kaye, W., Mehta, P., Horton, D.K., 2018. Amyotrophic lateral sclerosis mortality in the United States, 2011-2014. Neuroepidemiology 51 (1–2), 96–103.

Lee, Y., Messing, A., Su, M., Brenner, M., 2008. GFAP promoter elements required for region-specific and astrocyte-specific expression. Glia 56 (5), 481–493.

Liddelow, S.A., Guttenplan, K.A., Clarke, L.E., Bennett, F.C., Bohlen, C.J., Schirmer, L., Bennett, M.L., Munch, A.E., Chung, W.S., Peterson, T.C., Wilton, D.K., Frouin, A., Napier, B.A., Panicker, N., Kumar, M., Buckwalter, M.S., Rowitch, D.H., Dawson, V. L., Dawson, T.M., Stevens, B., Barres, B.A., 2017. Neurotoxic reactive astrocytes are induced by activated microglia. Nature 541 (7638), 481–487.

Liu, J., Wang, F., 2017. Role of Neuroinflammation in amyotrophic lateral sclerosis: cellular mechanisms and therapeutic implications. Front. Immunol. 8, 1005.

Morchikh, M., Cribier, A., Raffel, R., Amraoui, S., Cau, J., Severac, D., Dubois, E., Schwartz, O., Bennasser, Y., Benkirane, M., 2017. HEXIM1 and NEAT1 long non-coding RNA form a multi-subunit complex that regulates DNA-mediated innate immune response. Mol. Cell 67 (3), 387–399 e5.

Murayama, G., Chiba, A., Kuga, T., Makiyama, A., Yamaji, K., Tamura, N., Miyake, S., 2020. Inhibition of mTOR suppresses IFNalpha production and the STING pathway in monocytes from systemic lupus erythematosus patients. Rheumatology (Oxford) 59 (10), 2992–3002.

Nagai, M., Re, D.B., Nagata, T., Chalazonitis, A., Jessell, T.M., Wichterle, H., Przedborski, S., 2007. Astrocytes expressing ALS-linked mutated SOD1 release factors selectively toxic to motor neurons. Nat. Neurosci. 10 (5), 615–622.

Nasiri, E., Sankowski, R., Dietrich, H., Oikonomidi, A., Huerta, P.T., Popp, J., Al-Abed, Y., Bacher, M., 2020. Key role of MIF-related neuroinflammation in neurodegeneration and cognitive impairment in Alzheimer's disease. Mol. Med. 26 (1), 34.

Papadeas, S.T., Kraig, S.E., O'Banion, C., Lepore, A.C., Maragakis, N.J., 2011. Astrocytes carrying the superoxide dismutase 1 (SOD1G93A) mutation induce wild-type motor neuron degeneration in vivo. Proc. Natl. Acad. Sci. USA 108 (43), 17803–17808.

Pei, F., Ma, L., Jing, J., Feng, J., Yuan, Y., Guo, T., Han, X., Ho, T.V., Lei, J., He, J., Zhang, M., Chen, J.F., Chai, Y., 2023. Sensory nerve niche regulates mesenchymal stem cell homeostasis via FGF/mTOR/autophagy axis. Nat. Commun. 14 (1), 344.

Perez-Riverol, Y., Bai, J., Bandla, C., Garcia-Seisdedos, D., Hewapathirana, S., Kamatchinathan, S., Kundu, D.J., Prakash, A., Frericks-Zipper, A., Eisenacher, M., Walzer, M., Wang, S., Brazma, A., Vizcaino, J.A., 2022. The PRIDE database resources in 2022: a hub for mass spectrometry-based proteomics evidences. Nucleic Acids Res. 50 (D1), D543–D552.

Powell, J.D., Pollizzi, K.N., Heikamp, E.B., Horton, M.R., 2012. Regulation of immune responses by mTOR. Annu. Rev. Immunol. 30, 39–68.

Pramatarova, A., Laganiere, J., Roussel, J., Brisebois, K., Rouleau, G.A., 2001. Neuron-specific expression of mutant superoxide dismutase 1 in transgenic mice does not lead to motor impairment. J. Neurosci. 21 (10), 3369–3374.

Raoul, C., Abbas-Terki, T., Bensadoun, J.C., Guillot, S., Haase, G., Szulc, J., Henderson, C. E., Aebischer, P., 2005. Lentiviral-mediated silencing of SOD1 through RNA interference retards disease onset and progression in a mouse model of ALS. Nat. Med. 11 (4), 423–428.

Reischauer, C., Gutzeit, A., Neuwirth, C., Fuchs, A., Sartoretti-Schefer, S., Weber, M., Czell, D., 2018. In-vivo evaluation of neuronal and glial changes in amyotrophic lateral sclerosis with diffusion tensor spectroscopy. Neuroimage Clin 20, 993–1000.

Rinsch, C., Quinodoz, P., Pittet, B., Alizadeh, N., Baetens, D., Montandon, D., Aebischer, P., Pepper, M.S., 2001. Delivery of FGF-2 but not VEGF by encapsulated

genetically engineered myoblasts improves survival and vascularization in a model of acute skin flap ischemia. Gene Ther. 8 (7), 523–533.
Rochat, C., Bernard-Marissal, N., Kallstig, E., Pradervand, S., Perrin, F.E., Aebischer, P., Raoul, C., Schneider, B.L., 2022. Astrocyte-targeting RNA interference against mutated superoxide dismutase 1 induces motoneuron plasticity and protects fast-fatigable motor units in a mouse model of amyotrophic lateral sclerosis. Glia 70 (5), 842–857.
Rohart, F., Gautier, B., Singh, A., Le Cao, K.A., 2017. mixOmics: an R package for 'omics feature selection and multiple data integration. PLoS Comput. Biol. 13 (11), e1005752.
Rothstein, J.D., Patel, S., Regan, M.R., Haenggeli, C., Huang, Y.H., Bergles, D.E., Jin, L., Dykes Hoberg, M., Vidensky, S., Chung, D.S., Toan, S.V., Bruijn, L.I., Su, Z.Z., Gupta, P., Fisher, P.B., 2005. Beta-lactam antibiotics offer neuroprotection by increasing glutamate transporter expression. Nature 433 (7021), 73–77.
Roybon, L., Lamas, N.J., Garcia, A.D., Yang, E.J., Sattler, R., Lewis, V.J., Kim, Y.A., Kachel, C.A., Rothstein, J.D., Przedborski, S., Wichterle, H., Henderson, C.E., 2013. Human stem cell-derived spinal cord astrocytes with defined mature or reactive phenotypes. Cell Rep. 4 (5), 1035–1048.
Savchenko, E., Teku, G.N., Boza-Serrano, A., Russ, K., Berns, M., Deierborg, T., Lamas, N. J., Wichterle, H., Rothstein, J., Henderson, C.E., Vihinen, M., Roybon, L., 2019. FGF family members differentially regulate maturation and proliferation of stem cell-derived astrocytes. Sci. Rep. 9 (1), 9610.
Siddique, T., Ajroud-Driss, S., 2011. Familial amyotrophic lateral sclerosis, a historical perspective. Acta Myol 30 (2), 117–120.
Son, J., Tae, J.Y., Min, S.K., Ko, Y., Park, J.B., 2020. Fibroblast growth factor-4 maintains cellular viability while enhancing osteogenic differentiation of stem cell spheroids in part by regulating RUNX2 and BGLAP expression. Exp. Ther. Med. 20 (3), 2013–2020.
Song, L., Wang, L., Hou, Y., Zhou, J., Chen, C., Ye, X., Dong, W., Gao, H., Liu, Y., Qiao, G., Pan, T., Chen, Q., Cao, Y., Hu, F., Rao, Z., Chen, Y., Han, Y., Zheng, M., Luo, Y., Li, X., Chen, Y., Huang, Z., 2022. FGF4 protects the liver from nonalcoholic fatty liver disease by activating the AMP-activated protein kinase-caspase 6 signal axis. Hepatology 76 (4), 1105–1120.
Stoklund Dittlau, K., Terrie, L., Baatsen, P., Kerstens, A., De Swert, L., Janky, R., Corthout, N., Masrori, P., Van Damme, P., Hyttel, P., Meyer, M., Thorrez, L., Freude, K., Van Den Bosch, L., 2023. FUS-ALS hiPSC-derived astrocytes impair human motor units through both gain-of-toxicity and loss-of-support mechanisms. Mol. Neurodegener. 18 (1), 5.
Su, T., Huang, L., Zhang, N., Peng, S., Li, X., Wei, G., Zhai, E., Zeng, Z., Xu, L., 2020. FGF14 functions as a tumor suppressor through inhibiting PI3K/AKT/mTOR pathway in colorectal Cancer. J. Cancer 11 (4), 819–825.
Sui, H., Hao, M., Chang, W., Imamichi, T., 2021. The role of Ku70 as a cytosolic DNA sensor in innate immunity and beyond. Front. Cell. Infect. Microbiol. 11, 761983.
Takahama, M., Fukuda, M., Ohbayashi, N., Kozaki, T., Misawa, T., Okamoto, T., Matsuura, Y., Akira, S., Saitoh, T., 2017. The RAB2B-GARIL5 complex promotes cytosolic DNA-induced innate immune responses. Cell Rep. 20 (12), 2944–2954.
Tan, H.Y., Yong, Y.K., Xue, Y.C., Liu, H., Furihata, T., Shankar, E.M., Ng, C.S., 2022. cGAS and DDX41-STING Mediated Intrinsic Immunity Spreads Intercellularly to Promote Neuroinflammation in SOD1 ALS Model. iScience 25 (6), 104404.
Tripathi, P., Rodriguez-Muela, N., Klim, J.R., de Boer, A.S., Agrawal, S., Sandoe, J., Lopes, C.S., Ogliari, K.S., Williams, L.A., Shear, M., Rubin, L.L., Eggan, K., Zhou, Q., 2017. Reactive astrocytes promote ALS-like degeneration and intracellular protein aggregation in human motor neurons by disrupting autophagy through TGF-beta1. Stem Cell Rep. 9 (2), 667–680.
van Bilsen, J.H.M., Dulos, R., van Stee, M.F., Meima, M.Y., Rouhani Rankouhi, T., Neergaard Jacobsen, L., Staudt Kvistgaard, A., Garthoff, J.A., Knippels, L.M.J., Knipping, K., Houben, G.F., Verschuren, L., Meijerink, M., Krishnan, S., 2020. Seeking windows of opportunity to shape lifelong immune health: a network-based strategy to predict and prioritize markers of early life immune modulation. Front. Immunol. 11, 644.
Vance, C., Rogelj, B., Hortobagyi, T., De Vos, K.J., Nishimura, A.L., Sreedharan, J., Hu, X., Smith, B., Ruddy, D., Wright, P., Ganesalingam, J., Williams, K.L., Tripathi, V., Al-Saraj, S., Al-Chalabi, A., Leigh, P.N., Blair, I.P., Nicholson, G., de Belleroche, J., Gallo, J.M., Miller, C.C., Shaw, C.E., 2009. Mutations in FUS, an RNA processing protein, cause familial amyotrophic lateral sclerosis type 6. Science 323 (5918), 1208–1211.
Writing, G., Edaravone, A.L.S.S.G., 2017. Safety and efficacy of edaravone in well defined patients with amyotrophic lateral sclerosis: a randomised, double-blind, placebo-controlled trial. Lancet Neurol. 16 (7), 505–512.
Xie, Y., Su, N., Yang, J., Tan, Q., Huang, S., Jin, M., Ni, Z., Zhang, B., Zhang, D., Luo, F., Chen, H., Sun, X., Feng, J.Q., Qi, H., Chen, L., 2020. FGF/FGFR signaling in health and disease. Signal Transduct. Target. Ther. 5 (1), 181.
Xue, X., Wu, J., Ricklin, D., Forneris, F., Di Crescenzio, P., Schmidt, C.Q., Granneman, J., Sharp, T.H., Lambris, J.D., Gros, P., 2017. Regulator-dependent mechanisms of C3b processing by factor I allow differentiation of immune responses. Nat. Struct. Mol. Biol. 24 (8), 643–651.
Yamanaka, K., Chun, S.J., Boillee, S., Fujimori-Tonou, N., Yamashita, H., Gutmann, D.H., Takahashi, R., Misawa, H., Cleveland, D.W., 2008. Astrocytes as determinants of disease progression in inherited amyotrophic lateral sclerosis. Nat. Neurosci. 11 (3), 251–253.
Yu, C.H., Davidson, S., Harapas, C.R., Hilton, J.B., Mlodzianoski, M.J., Laohamonthonkul, P., Louis, C., Low, R.R.J., Moecking, J., De Nardo, D., Balka, K.R., Calleja, D.J., Moghaddas, F., Ni, E., McLean, C.A., Samson, A.L., Tyebji, S., Tonkin, C.J., Bye, C.R., Turner, B.J., Pepin, G., Gantier, M.P., Rogers, K.L., McArthur, K., Crouch, P.J., Masters, S.L., 2020. TDP-43 triggers mitochondrial DNA release via mPTP to activate cGAS/STING in ALS. Cell 183 (3), 636–649 e18.
Zhang, Y., Yu, Z., Ye, N., Zhen, X., 2023. Macrophage migration inhibitory factor (MIF) in CNS diseases: functional regulation and potential therapeutic indication. Fundamental Research.
Zhao, R.Z., Jiang, S., Zhang, L., Yu, Z.B., 2019. Mitochondrial electron transport chain, ROS generation and uncoupling (review). Int. J. Mol. Med. 44 (1), 3–15.
Zhao, C., Devlin, A.C., Chouhan, A.K., Selvaraj, B.T., Stavrou, M., Burr, K., Brivio, V., He, X., Mehta, A.R., Story, D., Shaw, C.E., Dando, O., Hardingham, G.E., Miles, G.B., Chandran, S., 2020. Mutant C9orf72 human iPSC-derived astrocytes cause non-cell autonomous motor neuron pathophysiology. Glia 68 (5), 1046–1064.
Ziff, O.J., Clarke, B.E., Taha, D.M., Crerar, H., Luscombe, N.M., Patani, R., 2022. Meta-analysis of human and mouse ALS astrocytes reveals multi-omic signatures of inflammatory reactive states. Genome Res. 32 (1), 71–84.